Teresa Flores Coimbra

Investigação de parâmetros da emissão térmica em comprimentos de onda rádio como sonda da energia dos raios gama em novas clássicas

The investigation of thermal emission parameters at radio wavelengths as a probe for gamma-ray energies in classical novae

Teresa Flores Coimbra

Investigação de parâmetros da emissão térmica em comprimentos de onda rádio como sonda da energia dos raios gama em novas clássicas

The investigation of thermal emission parameters at radio wavelengths as a probe for gamma-ray energies in classical novae

Dissertação apresentada à Universidade de Aveiro para cumprimento dos requesitos necessários à obtenção do grau de Mestre em Física, realizada sob a orientação científica do Doutor Valério Alípio Roberts Machado Ribeiro, Investigador Auxiliar do Instituto de Telecomunicações

o júri / the jury

presidente / president

Prof. Doutor Vitor Hugo da Rosa Bonifácio
Professor Auxiliar do Departamento de Física da Universidade de Aveiro

vogais / examiners committee

Doutor Valério Alípio Roberts Machado Ribeiro
Investigador Auxiliar do Instituto de Telecomunicações (orientador)

Prof. Doutor Marcos Perez Diaz
Prof. Livre-Docente do Instituto de Astronomia, Geofísica e Ciências Atmosféricas da Universidade de São Paulo

agradecimentos /
acknowledgements

To my adviser, who was always available and supportive during this endeavor, as well as for his unwavering understanding when life intervened.

To all of my close friends for making this an unforgettable experience and for being there with me through the highs and lows. To all of my close acquaintances, for their kind words, which have helped me more than they can realize.

To my close family for their unconditional support and for enabling me to take my time and focus on myself and my education.

To my psychologist, who helped me get to the point where I'm strong enough to take on this challenge.

To every woman who has walked this field before and paved the road for me.

And to me, who persisted when things got hard.

Obrigada!

Our thanks to Laura Chomiuk and the e-nova group for making the VLA observations readily available.

The calculations, in this dissertation, were carried out at the OBLIVION Supercomputer (based at the High Performance Computing Center - University of Évora) funded by the ENGAGE SKA Research Infrastructure (reference POCI-01-0145-FEDER-022217 - COMPETE 2020 and the Foundation for Science and Technology, Portugal) and by the BigData@UE project (reference ALT20-03-0246-FEDER-000033 - FEDER and the Alentejo 2020 Regional Operational Program).

Palavras-Chave

Novas Clássicas, Radio Continuum: Geral, Gamma-Rays Continuum: Geral

Resumo

O estudo de novas clássicas nas últimas duas décadas tem mudado rapidamente devido à melhoria de telescópios rádio, como o Karl Janky Very Large Array e novos telescópios espaciais de raios γ, como o Fermi. Estudos de multi-frequências destes objetos são capazes de fornecer informação detalhada sobre as condições físicas durante erupções, permitindo o estudo das contribuições de novas no meio interestelar. Prevê-se que algumas, senão todas, as novas clássicas emitam raios γ com energia na ordem dos GeV. No entanto, a origem destas emissões não está ainda totalmente compreendida. Contudo, existe indicações significativas de que estão relacionadas com choques internos dentro do material expelido, que também causa emissão não-térmica e produção de poeira.

Neste estudo, curvas de luz nas bandas de rádio de 7 novas clássicas (V959 Mon, V1323 Sco, V5668 Sgr, V357 Mus, V906 Car, V5589 Sgr e V1723 Aql) foram ajustadas com um modelo de emissão térmica com simetria esférica, dos quais 2 são de dados não publicados (V5590 Sgr e V357 Mus). O modelo é baseado no "Hubble Flow Model" e está acoplado ao código de Monte Carlo de Cadeias de Markov, `emcee`. Esta é a primeira vez que o código `emcee` foi acoplado para fazer ajustes de curvas de luz nas bandas de rádio de novas. Emissão não-térmica estava claramente evidente nos resultados dos ajustes, como era de esperar tendo em conta resultados de estudos prévios. Em 6 de 7 novas, o modelo foi capaz de dissociar as duas componentes de emissão.

De 7 novas, apenas 5 foram detetadas em emissão de raios γ. Nesta dissertação pretende-se identificar conexões entre os parâmetros de entrada da radiação térmica (distância, fator de preenchimento, velocidade máxima de expansão e massa expelida) e o brilho de raios γ, ou o limite de não deteção. Até à data, tentativas para encontrar correlações entre parâmetros a diferentes comprimentos de onda e emissão de raios γ, ou falta dela, tiveram diversos graus de sucesso. Nós encontrámos uma correlação inversa entre a massa ejetada e a luminosidade de raios γ. Esta correlação inversa é remanescente da atenuação de fotões γ, por uma barreira absorvente (muito provavelmente o próprio material ejetado).

A correlação inversa encontrada entre a emissão de raios γ e a massa expelida pode também ajudar a explicar o fator de 10^2 observado nos valores de luminosidade de raios γ.

Keywords Classical Novae, Radio Continuum: General; Gamma-Rays Continuum: General

Abstract

The study of Classical Novae over the last two decades has fastly changed due to the upgrade of radio telescopes, such as the Karl Jansky Very Large Array, and the advent of space-based γ-ray telescopes, such as Fermi. Multi-frequency studies of these objects are able to provide us detailed information about the physical conditions after eruptions enabling us to study the contributions of novae to their interstellar medium. Some, if not all, classical novae are predicted to release GeV γ-rays, although the origin of these emissions is yet to be fully understood. However, there are significant indications that it is connected to internal shocks within the ejected material, which also causes the non-thermal emission and dust production.

The radio light curves of 7 classical novae (V959 Mon, V1324 Sco, V5668 Sgr, V357 Mus, V906 Car, V5589 Sgr, and V1723 Aql) were fitted with a spherically symmetric thermal emission model in this study, of which 2 are from previously unpublished data (V5668 Sgr and V357 Mus). The model is based on the "Hubble Flow Model" and is coupled with the Markov Chain Monte Carlo (MCMC) code, `emcee`. This is the first time the `emcee` code was coupled to fit radio light curves of novae. Non-thermal emission was clearly evident in the results of the fit, as expected from previous studies of these novae. In 6 out of the 7 novae the model was capable to decouple the two components of the emission.

Of the 7 novae, only 5 were detected with γ-ray emission. This dissertation aims to identify connections between the thermal emission input parameters (distance, filling factor, maximum expansion velocity, and mass of ejecta) and the γ-ray brightness or the limit of non-detection. To date, attempts to find correlations between parameters at different wavelengths and γ-ray emission, or lack of, were met with various successes. We find an inverse correlation between the ejecta mass and the γ-ray luminosity. This inverse correlation is reminiscent of the attenuation of γ-ray photons by an absorbing screen (most likely the ejecta itself).

The inverse correlation found between the γ-ray emission and ejected mass may also help explain the origin of the 10^2 factor observed in the values of detected γ-ray luminosity.

Contents

List of Figures

List of Tables

Introduction

Radio observations are extremely useful in nova research since they provide information on a variety of elements of the eruption, including distance to the nova, total ejected mass, kinetic energy, and ejecta density profile. In particular, the ejecta mass is a key prediction of the nova models, allowing them to be directly tested. Resolved radio images are also useful to provide an image of the structure of the ejecta, in some cases showing evidence for multiple outflows [4]. In addition, radio emission has the advantage of not being subject to extinction by dust and evolving on timescales of years, compared to other wavelengths.

Until recently, we regarded clasical novae (CNe) radio emission as mostly thermal, due to thermal *bremsstrahlung* from the ejecta, and most radio data fitting models assume solely this emission. Non-thermal emission was first anticipated exclusively for novae with a red-giant partner and high-density winds, when shocks from the companion's wind were expected [5]. Today's scientific agreement is that all novae release both thermal and non-thermal radiation, just in different amounts.

Current observations suggest that shocks are common in CNe, even those without a companion's wind with what to shock. The internal shock model was proposed to explain these previously unexpected shocks. In this model, shocks occur within the ejecta due to colisions of different components with different phases of mass ejection [6, 7]. This concept was first developed to explain the unique behavior of the nova V959 Mon based on resolved radio imaging [8] however, research suggests that the existence of at least two physically distinct flows is common in many other CNe [4].

These shocks could explain the origin of non-thermal emission, which we observe through multiple peaked radio light curves and high brightness temperatures that characterize this type of emission [7,9]. Other relevant signs of shocks are the formation of dust in environments where it should be suppressed [10] and the emission of γ-ray and the two-order-of-magnitude variation in its luminosity [11].

So far, γ-rays have been detected in fifteen CNe, some of which do not appear to be embedded in the companion's wind or to be recurrent novae, supporting the internal shock theory [7,8]. A number of authors have attempted to correlated different observable measures to the gamma-ray brightness without much success [12].

In our study we focused on the radio light curves of 7 classical novae (V959 Mon, V1324 Sco, V5668 Sgr, V357 Mus, V906 Car, V5589 Sgr, and V1723 Aql). We used a thermal model based on the "Hubble Flow Model" to fit the curves and derive some nova and ejecta parameters (distance, filling factor, maximum expansion velocity, and ejecta mass). We coupled the thermal emission model with an MCMC code, `emcee`, that allowed us to retrieve confidence limits. This is the first time the `emcee` code has been used to fit radio light curves of novae. The MCMC approach is superior than generic Monte Carlo algorithms at solving multi-dimensional problems, and the `emcee` code, in particular, allows us to take use of a computing cluster since it utilizes an ensemble of walkers moved in parallel [13, 14].

In addiction to the best fitting model, we also calculate and represent graphically the

brightness temperature, the residuals and the spectral index for both the measured fluxes and for the residual fluxes.

In none of the novae, our model provided an acceptable fit for the complete light curve. It tends to behave better at later times, when the non-thermal component of the emission is reduced and the ejecta is beginning to become optically thin. This is due to the fact that the novae analyzed in this study display evidence of non-thermal emission, such as an excess of emission relative to the thermal model prediction, high brightness temperatures, and multiple-peaked radio light curves. In 6 out of the 7 novae a non-thermal component is very clear when we remove the thermal component predicted by the model. We find that the non-thermal component is more dominant at lower frequencies, and we establish that it is the predominant emission mechanism in radio wavelengths over the first 100 days in most of the novae studied.

In the γ-ray wavelength, only 5 of the 7 novae analyzed have been detected. We discover a promising correlation between the best fit parameters for each novae and its γ-ray brightness or the limit of non-detection: γ-ray luminosities appear to be inversely correlated with ejecta masses. This behavior is the opposite of what the internal shock model [12] predicts.

We propose that the drop in γ-ray luminosity with increasing ejecta mass is due to attenuation by dense material within the ejecta. This suggests that the location of the origin ofγ-rays must be reconsidered. We offer a preliminary fit of an exponential decay, showing results that invite further studies.

Dissertation Outline

We present the theoretical background in the *first chapter* in order to acquaint the reader with the state-of-the-art and motivation for this dissertation. In the *second chapter* we present the methods utilized to generate the results provided and discussed in *chapter three*. The *last chapter* summarizes the major findings of this investigation and leaves suggestions for future work.

Chapter 1

Theoretical Background

A nova (derived from the Latin *stella nova*, or new star) is a type of Cataclysmic Variable (CV) star, that is, a binary star system that undergoes a sudden increase in brightness. The typical classical nova (CN - singular; CNe - plural) system is composed of a White Dwarf (WD) with a core rich in either nickel (Ni), carbon (C) and oxygen (O), or O, neon (Ne) and magnesium (Mg) and a secondary companion, generally a cooler lower mass main-sequence star. When the binary stars are close enough, there is mass transfer from the secondary star to the surface of the WD via an accretion disk that surrounds the WD. This leads to a build-up of material which can erupt as a Thermonuclear Runaway Reaction (TNR), producing radiation that can be observed in all the bands of the electromagnetic spectrum, from radio to γ-rays. Novae are the third most energetic eruptions in the Universe after γ-ray bursts and supernovae [15] but are far more frequent in a given galaxy than these.

As the hydrogen-rich matter accumulates at the base of the WD, it is gradually compressed and heats the material underneath it which becomes degenerate due to the increasing pressure. At a critical temperature of $\sim 10^6$ K and a critical pressure of $\sim 10^{19}$ N m^{-2}, nuclear fusion reactions near the bottom of the accreted layers restart. Two mechanisms operate on the nuclear reactions depending on the temperature [16]: the proton-proton chain reaction and the Carbon-Nitrogen-Oxygen (CNO) cycles. Although the former reactions are important during the accretion phase of the eruption, it is the CNO cycles that power the final stages of the TNR and the evolution to the peak of the eruption. Both nuclear reactions raise the temperature of the accreted material. Since in degenerate matter the pressure is solely dependent on density, it cannot expand to moderate the burning rate. The temperature and the nuclear energy generation rate increase continuously, driving a TNR. Eventually, the eruption occurs with a sudden visual brightening at optical wavelength. This brightening lasts for a period of hours to days and is followed by a slow decline in brightness over the next few weeks to months. During the eruption, a average of 2×10^{-4} M$_\odot$ of material is expelled [1] at velocities that can exceed 10^3 km s^{-1} [17, 18].

Various simulations of nova eruptions have shown that the behavior of CNe eruptions is dependent on only three independent parameters: the WD mass, the WD temperature (or luminosity or age) and the mass accretion rate from the companion [18, 19]. In reality, novae show a diversity of behaviors in multiple wavelengths that cannot be explained by just these three factors. However, shocks and complex mass ejection, as will be discussed on section 1.4, may be able to explain some of these behaviors.

It is though that the first recorded CNe observation was recorded over 3000 years ago, given the Far Eastern writings and the estimated rate of nova eruptions [20]. Since then, over 1000 novae have been detected [21], with about 400 of them in the Milky Way [22]. The rate of these eruptions in our galaxy is estimated to be of 50 per year, but a rate of 100

per year is not ruled out [23]. Despite this, the observed rate is substantially lower than the above-mentioned estimate, with only approximately 10 observations each year, possibly due to Sun interference, star crowding in the galactic center region, and dust obscuration [24].

Galactic novae are separated into two groups based on the spectroscopic and photometric properties [25]: the fast and bright novae confined to a height z of less than 100 pc above the Galactic plane and the slow and dim novae located in the Galactic bulge (up to $z \sim$ 1000 pc) [26]. This distribution may be understood if we consider that, since fast novae are inherently more luminous, they are more likely to form from higher mass WDs which are more abundant in the disk than in the bulge [26].

1.1 Recurrent Novae

Since the WD is not destroyed, the accretion begins again, leading to repeated eruptions. If the recurrence happens on timescales short enough for humans to observe, then the novae are referred to as Recurrent Novae (RNe), in opposition to the CNe. The secondary star in these novae is usually a red giant and not a star close to the main sequence as in CNe [27] and the primary star is believed to be massive, with the mass being close to the Chandrasekhar limit[1] in most systems [18, 28]. RNe are also shorter in eruption duration and usually have longer orbital periods [29].

A significant fraction of RNe eruptions are thought to be missed due to their shorter eruptions which can easily fit into the solar and lunar gaps [29]. Studies of the demographics of the nova population point towards approximately 25% of CNe actually being RNe for which only one eruption has been discovered [30]. The short timescale for the recurrence of the nova eruption is caused by two characteristics of the system: a high-mass WD and a high accretion rate. The more massive the WD is, higher is the surface gravity, and therefore smaller is the amount of accreted mass needed before the TNR is triggered. A higher accretion rate implies that it takes a shorter time period for the matter to accumulate and reach the needed pressure to trigger the TNR [18].

If the ejected mass is less than that accreted since the last eruption, then the WD will grow in mass over time and either form a neutron star or evolve towards explosion as a Type Ia supernova (SNe Ia). The composition, mass, as well as the accretion rate and ejected mass, will decide if the WD will reach the Chandrasekhar limit [31]. Observational results from the eruptions of the well-studied RNe RS Oph find no evidence of mass growth [18] but studies of the mass distribution of WD in CVs show that they are statistically more massive than those in single WDs [32, 33].

Supernovae (SNe) are the result of the explosive death of a star. These events can be caused by the collapse of the core of a massive star or by a massive WD undergoing a thermonuclear explosion, the SNe Ia. The latter is especially interesting to astrophysicists and cosmologists because they constitute "standardizable candles" and can be used to estimate cosmological distances, unlike core-collapse supernovae [34, 35]. The origin of these powerful stellar explosions is yet to be fully understood. Thus, studying novae can give important clues to the understanding of the origins of these events.

Several other questions remain to support the model that these SNe evolve from RNe. The two main are if there is a sufficient population of RNe to account for the observed rate of SNe Ia and why so far no radio emission has been detected coming from this type of SNe [36, 37].

[1]The Chandrasekhar limit is the maximum mass of a stable white dwarf star, corresponding to a mass of more than 1.44 times that of the Sun

1.2 Optical Emission

The typical optical light-curve evolution is shown in Figure 1.1. It starts with a sudden rise to maximum by several orders of magnitude in a matter of hours to a few days. The rising time depends on the speed of each nova (Table 1.1). This rise happens without warning, so unless it has been in the field of sky surveys and large area telescopes, this rise is not observed [38]. In the light curve of the majority of novae, there is a flattening, known as the pre-maximum halt, about 1-2 magnitudes below maximum.

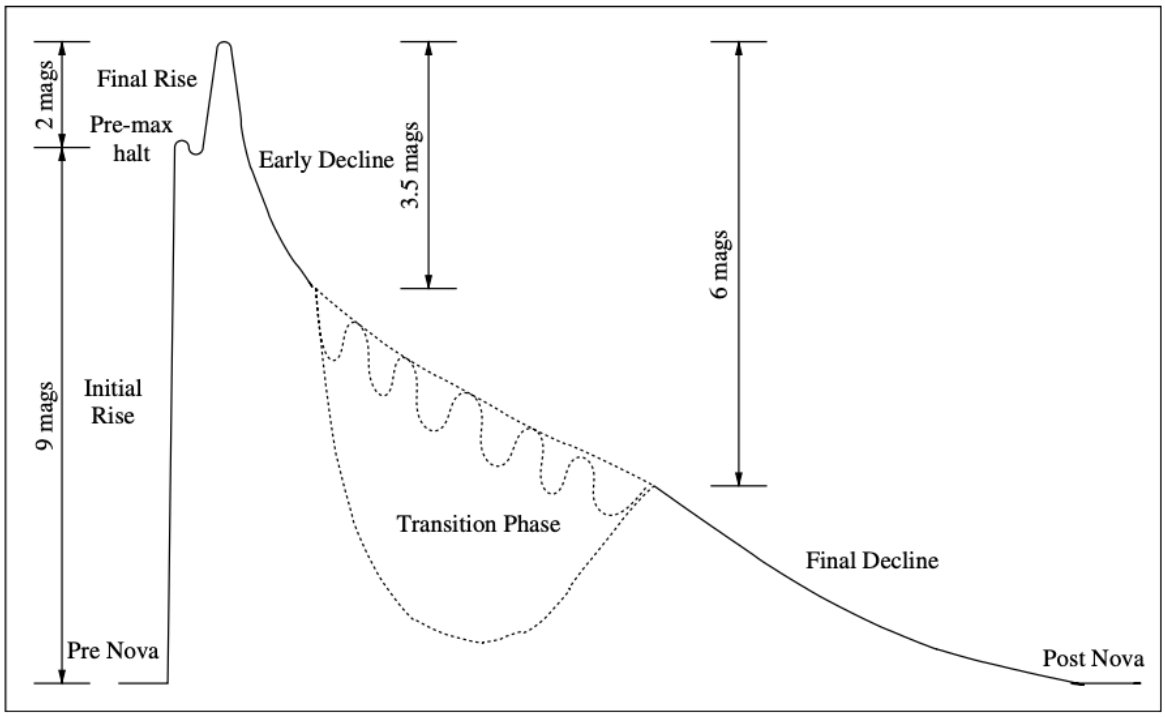

Figure 1.1: The idealized nova optical light curve with the horizontal axis representing time and the vertical axis representing the magnitude of the optical light. The duration and particular behavior of each phase of the curve is explained in the accompanying text. Reproduced from [1].

Novae remain at maximum brightness for a few hours or days, depending on the speed of the nova, followed by decline. Fast novae have usually a smooth early decline, while slow novae tend to display oscillations in brightness during that period.

Various attempts were made to create a system of classification of novae based on the structure of the optical curve. Their rate of decline can be characterized by t_2 and t_3, the times taken for their brightness to decay by 2 and 3 orders of magnitudes from the peak, respectively. The faster novae (smaller t_2 and t_3) have higher ejection velocities and a higher peak in the absolute magnitude [26]. The most used classification system is the one of Payne-Gaposchkin [3] which is based on the decline time t_2 and separates novae into 5 speed-classes with different decline rates (Table 1.1).

After a decline of 3.5 magnitudes following the maximum peak, the Transition Phase takes place. Some novae display no oscillation during this period, while other display interesting behaviors, mostly periodic or quasi-periodic oscillations up to 1.5 mag on timescales of the order of a few days, or a deep drop down for months due to the formation of dust in the ejecta. The later phenomena happen because the dust absorbs much of the optical emission,

Table 1.1: Payne-Gaposchkin's System of Speed Classes of Classical Novae [3].

Speed Class	t_2 (days)	Rate of Decline (mag/day)
Very Fast	10 or less	>0.20
Fast	11 to 25	0.18 to 0.08
Moderately Fast	26 to 80	0.07 to 0.025
Slow	80 to 150	0.024 to 0.013
Very Slow	151 to 250	0.012 to 0.008

re-emitting it at infrared (IR) wavelengths.

The final decline from about 6 mag below maximum lasts on the order of a few years until the brightness returns to pre-nova levels, known as quiescence. During this decline the drop in optical flux is counterbalanced by an increase in the flux on higher wavelengths. Therefore, the bolometric luminosity of the nova remains roughly constant, which is consistent with the fact that the WD continues to burn residual hydrogen steadily after the eruption.

1.3 Radio Emission

Nova eruptions at radio wavelengths evolve more slowly, on timescales of years, rather than the months observed at optical wavelengths. Furthermore, radio wavelengths do not suffer from interstellar extinction, unlike optical/IR or X-rays wavelengths, and are capable of reaching ground-based observatories unimpeded by the weather.

A nova shell starts as optically thick at all frequencies. During the early stages, the radio flux density has a spectral index of $\alpha > 0$. This index describes how the flux of an electromagnetic source changes with frequency, such that $S_\nu \propto \nu^\alpha$ where S is the flux density and ν is the observed frequency.

Eventually the flux density reaches its maximum, its optical depth (τ) equals one and the emission is dominated by visible light. This quantity τ is a measure of how opaque an emitting material is to its own radiation - if $\tau > 1$, the material is said to be optically thick, while for $\tau < 1$ it is optically thin.

The time when this peak is reached depends on the mass and the velocity of the ejecta, while the behavior of the turnover (duration on time and dependency on frequency) is proportional to the size of the emitting shell. This is why radio observations are particularly useful at estimating these parameters.

As the ejecta expands, the density drops, and we can see farther into the ejecta. The radio frequency emission starts to penetrate through part of the shell, beginning with the highest frequencies first, so emission at higher frequencies emerges from deeper in the ejecta and evolves more rapidly [12].

Until recently we thought of CNe radio emission as mostly thermal emission. This thermal (or free-free) emission in novae is due to the thermal *bremsstrahlung* from the ejecta. This phenomena happens when a traveling electron interacts with an ion and experiences an acceleration, releasing energy through an electromagnetic wave. These ions are present as a result of the WD's photo-ionization of the ejecta. When an electron collides with an ion, it produces a very energetic emission with an X-ray wavelength. If the electron is only slightly deflected by a neighboring ion, radio emission occurs. When another electron comes into contact with that wave, it absorbs it, increasing its speed and energy. This is why ejecta turns transparent in visible wavelengths months before it does in IR and radio wavelengths.

The thermal radio emission detected at Earth depends on the ratio of free-free absorption and emission that occurs.

The commonly used models to fit radio data assume only thermal emission. The other assumption is a spherically symmetric shell with a density profile of the form

$$\rho = \frac{A}{r^p} \tag{1.1}$$

where r is the radial component of the shell, A is a constant and p is an integer (p=2-3 is a good fit for most of the observations).

The three simplest and most used models are the "Hubble Flow Model", the variable wind model and a unified model that combines both. The model used to fit the thermal emission in this dissertation is the "Hubble Flow Model" and will be discussed in detail in section 2.1.

The "Hubble Flow Model" was one of the first developed and is successful in explaining the radio evolution of a series of sources [2]. The input parameters are only the distance, the ejecta temperature, the total ejected mass, the outer ejecta velocity and the velocity gradient. This model assumes that the ejection is instantaneous, the velocity of the ejecta increases linearly with radius and the same amount of mass is expelled at all velocities, which implies $p = 2$.

For the optically thick phase, the model predicts a t^2 rise and a spectral index of $\alpha = 2$, i.e. $S_\nu \propto t^2\nu^2$. In the transition from optically thick to optically thin, the prediction is a $t^{4/3}$ decline with $\alpha = 0.6$, i.e. $S_\nu \propto t^{4/3}\nu^{0.6}$. At the optically thin phase, the prediction is a t^{-3} decay with $\alpha = -0.1$, i.e. $S_\nu \propto t^{-3}\nu^{-0.1}$.

Unlike the previous model, the "Wind Model" [39] assumes that the mass is continuously and steadily being lost in a timeframe longer than the timescale of the radio light curve. This loss is being driven by a wind resulting from residual nuclear burning on the WD surface following the nova eruption. This way there is no inner hard edge in the shell.

There is observational evidence in some novae of prolonged periods of ejection [40] but an inner boundary is necessary to reproduce the behavior of radio light curves at large t. This makes this model more useful at modeling the behavior at optical or IR wavelengths, given that at these wavelengths the peak is reached at much earlier times, prior to the detachment of the shell from the star.

A different model, the "Unified Model" [41], was needed to explain the light curves and images of V1974 Cyg, the first nova to be observed in all bands of the electromagnetic spectrum [42]. The optical and radio observations showed signs of non-spherical symmetric ejecta and temperature gradients [1]. This model combines a wind at early times that lasts until $t \geq t_1$, the moment at which the nova ejecta will detach from the WD and leave a cavity at small radius (similar to the "Hubble Flow Model").

The previously described simple models have been useful in explaining the radio curves of many novae, however, there are still some striking discrepancies between the predictions and the observations.

One of the most significant, and currently unexplained, disagreement between theoretical and observational predictions is the ejected mass. The masses estimated through the fit of the light curves using these theoretical models can be up to an order of magnitude smaller than the observationally determined [43]. One possible explanation may be inhomogeneous or clumpy ejecta [44] or an aspherical shape of the ejecta and multiple emission regions [8,39,45]. The latter explanation is discussed in section 1.4.

One solution to the first problem is the adoption of a filling factor f which is used to scale the mass as deduced from the theoretical models[2]. This factor can be experimentally

[2]This filling factor is not the same as the one described in the following chapter and employed in our model.

measured by optical spectroscopy, with current observational analysis being consistent with filling factors of less than unity [12]. The clumping of the ejecta can be included in the models if we consider a correction factor $\mathcal{F}$ that modifies the mass-loss rate and the optical depth ratio [46]:

$$\mathcal{F} = \frac{[f + (1-f)(N_H/N_L)^2]}{[f + (1-f)(N_H/N_L)]^2} \tag{1.2}$$

where N_H and N_L are the number densities of the high and low density regions respectively and f, the filling factor, represents the probability that a given line of sight passes through the high density material if the clumps are randomly dispersed through the ejecta. The implementation of this factor would result in a smaller ejecta mass, longer optically thick phase and higher flux during the partially optically thick and optically thin phases [47, 48]. This clumpiness has already been observed in the shell of the nova V5668 Sgr, where small clumps were detected in high resolution images by the ALMA telescope [49].

Non-thermal emission was first discovered in novae with a red-giant companion and high-density winds, such as the recurrent nova RS Oph [5], where shocks with the wind of the companion were to be expected. It was only with V1370 Aql and QU Vul [50,51] that it was detected in novae with main-sequence companions. Every nova, we now believe, produces both thermal and non-thermal radiation, but in varying proportions.

This type of emission is caused by the magnetic environment in the ejecta, which causes a phenomenon known as magnetobremsstrahlung, or synchrotron emission. It happens when electrons are accelerated possibly to ultra-relativistic speeds and their path is bent by a magnetic field. As a result, they radiate in the radio frequency range.

Non-thermal emission is characterized by being highly polarized due to the magnetic field [52] and having a much higher brightness temperature than that achieved for thermal emission, which is around $\sim 10^4$ K [7, 9]. In this work we assume that any emission that produces a brightness temperature higher than 5×10^4 K cannot be due to thermal emission alone.

The brightness temperature T_b, a parameter that can be used as a proxy for surface brightness, represents the temperature of the optically thick thermal blackbody necessary to originate the measured flux:

$$T_b(\nu, t) = \frac{S_\nu(t) c^2 D^2}{2\pi k_b \nu^2 \left(v_{ej} t\right)^2} \tag{1.3}$$

where S_ν is the measured flux, D is the distance to the observer, t is the time since explosion, v_{ej} is the ejecta velocity, ν is the observing frequency, k_b is the Boltzmann constant and c is the speed of light.

The synchrotron emission is known as "non-thermal radiation" since it cannot be described by the spectrum of thermal *bremsstrahlung* (black-body radiation). The accelerated electrons have power-law energy distributions, such that $N(E) \propto E^{-p}$, where $N(E)$ is the number of electrons per unit volume with energy E and p is the power-law index.

When the radio source is optically thin ($\tau \ll 1$), the energies of the electrons are arbitrary and its spectrum is the superposition of the spectra generated from individual electrons.

We can consider the following approximation: each electron with a Lorentz factor γ in a magnetic field $\mathbf{B}$ radiates all of its energy at a single frequency, the critical frequency ν_c, which is given by:

The term filling factor in our case stands for the difference between the inner and outer radius of the ejecta and is represented by "*ff*".

$$\nu_c \approx \gamma^2 \nu_g = \left(\frac{E}{m_e c^2}\right)^2 \frac{e|\mathbf{B}|}{m_e 2\pi} \tag{1.4}$$

where ν_g is the (non-relativistic) cyclotron frequency given by $\nu_g = eB/m_e 2\pi$, with m_e corresponding to the rest mass of the electron and e its electrical charge.

The emission coefficient, that is the amount of energy emitted per unit volume, per unit time, per unit frequency, into a solid angle, can then be written as follows:

$$j(\nu)d\nu = \left(\frac{dE}{dt}\right) N(E)dE \tag{1.5}$$

considering that, from eq. (1.4), the energy E can be expressed as:

$$E = \gamma m_e c^2 = \left(\frac{\nu}{\nu_g}\right)^{1/2} m_e c^2 \tag{1.6}$$

and replacing its time derivative in eq. (1.5), we can express the emission coefficient in terms of $\nu, |\mathbf{B}|$, and fundamental constants:

$$j(\nu) \propto |\mathbf{B}|^{(p+1)/2}\, \nu^{(p-1)/2}. \tag{1.7}$$

Thermal and non-thermal emissions have different spectral indexes before and after the peak. After the peak, for a nova shell emitting only thermal radiation, the spectral index becomes almost flat with $\alpha \approx -0.1$. Contrastingly, we just concluded that in this phase synchrotron radiation has a spectral index of $\alpha = (p-1)/2$. Based on synchrotron emission in relativistic shocks of other astronomical phenomena, the typical value of α is between $\alpha = -0.5$ and $\alpha = -1$, which implies a value of p between 2 and 3. However, this low value of α is rarely measured in novae. Due to the negative spectral index, we expect a greater contribution of synchrotron radiation at lower frequencies.

To every emission process there must be an absorption process. In this case it's the synchrotron self-absorption. As we discussed before, the spectrum of synchrotron radiation emitted by a particle of energy E peaks around the critical frequency ν_c. We can then conclude that the emission and absorption processes at a given frequency ν are associated with electrons of roughly the same energy, and that only electrons with that energy will contribute to the emission and absorption at that frequency.

For a given frequency ν, the Lorentz factors of the associated electrons are approximately:

$$\gamma \approx \left(\frac{2\pi m_e \nu}{e|\mathbf{B}|}\right)^{1/2} \tag{1.8}$$

as seen from eq. (1.4).

For an ultrarelativistic gas, the energy in terms of the electron temperature T_e is given by $E = 3k_b T_e$. We can then write T_e as:

$$T_e \equiv \frac{E}{3k_b} = \frac{\gamma m_e c^2}{3k_b} \approx \left(\frac{2\pi m_e \nu}{e|\mathbf{B}|}\right)^{1/2} \frac{m_e c^2}{3k_b} \tag{1.9}$$

Thermodynamically, no thermal source can emit radiation of brightness temperature greater than its kinetic temperature. Because of that, the self-absorption effects become important at low frequencies when the T_b of the source approaches the T_e of the electrons emitting at that frequency and the source becomes optically thick ($\tau \gg 1$).

In the Rayleigh–Jeans limit ($h\nu \ll k_b T_e$), with h being Planck's constant, which is the relevant limit for any source that produces radio emission, T_b is given by:

$$T_b \equiv \frac{I_\nu c^2}{2k_b \nu^2} \tag{1.10}$$

where I_ν is the spectral brightness for the frequency ν.

Considering the point where $T_b \approx T_e$:

$$I_\nu = \frac{2k_b T_e \nu^2}{c^2} \tag{1.11}$$

and remembering from eq. (1.9) that $T_e \propto \nu^{1/2}$, we can arrive at:

$$I_\nu \propto \nu^{1/2}\nu^2 |\mathbf{B}|^{-1/2} = \nu^{5/2}|\mathbf{B}|^{-1/2} \tag{1.12}$$

Thus the low-frequency spectrum of an optically thick synchrotron source is a power law of slope 5/2 :

$$S(\nu) \propto \nu^{5/2} \tag{1.13}$$

Before the peak, for a shell emitting thermal emission the spectral index is $\alpha \leq 2$, lowering toward lower frequencies. Contrastingly, we just concluded that in a uniform magnetic field the spectral index for the non-thermal emission, $\alpha = 5/2$, therefore independent of the energy spectrum of the emitting electrons p.

1.4 Shocks in CNe and the Gamma-Ray Emission

Current observations show that shocks are ubiquitous in systems with a main-sequence primary, typically CNe, despite previously being only expected in systems with a red-giant primary or embedded in the wind of the companion. These, previously unexpected events, may be due to interactions within the ejecta when different components collide with one another (internal shocks), possibly due to different stages of mass ejection with different mass loss rates and outflow velocities [8].

The shocks may also be responsible for previously unexplained but frequently observed phenomena: variation in the duration of the optical peak [53], the detection of γ-ray at times nearly coincident with the optical peak [54] and the variation on its luminosity by at least two orders of magnitude [11], hard X-ray emission starting weeks to months after the outburst and multiple velocity components in the optical spectra [8]. Dense shocks are also an ideal environment for dust formation detected weeks to months after an outburst, when the harsh radiation from the WD surface should suppress it [10]. Further evidence comes from the signs of synchrotron radio emission, observed in the form of high brightness temperatures and multiple peaked radio light curves. The particular signs of this emission on the novae studied in this work are discussed case by case in chapter 3.1.

The high brightness temperatures (and other signs of shocks) can also be explained by a thermal mechanism: the photoionization heating of ejecta by the residual burning of nuclear fuel in the WD [55]. However, this type of heating would not produce brightness temperatures as high as the ones sometimes observed early in the eruption, when the ejecta is still optically thick and the produced photons can not go through the ejecta to the outer edges. Therefore, the high brightness temperature ($> 10^5$) sometimes observed this early in the evolution must be due to a mechanism happening near the photosphere of the ejecta.

Photoionization heating as the dominant emission mechanism was considered for some of the novae in this work but was discarded. Calculations of the temperature and volume of hot thermal plasma needed to achieve the emission observed excludes this mechanism (such as in V959 Mon [8] and V5589 Sag [56]). This heating would also produce X-ray emission that is sometimes not observed on these novae (such as in V1324 Sco [57]) and induce a lagging by several days between the detection of the produced γ-rays and the optical peaks, which is not observed either (such as in V906 Car [58]).

However, in order to generate internal shocks, some asymmetry in the mass ejection process is needed. The currently accepted model for internal shocks was initially proposed for the nova on V959 Mon as an explanation for the presence of γ-ray emission and for the evolution of the ejecta observed in the resolved radio imaging [8]. Ejecta images reveal two components extending from south-west to north-east at first, then a bipolar structure extending from east to west and finally a bipolar structure extending from north to south following a 90^{o} shift [59]. Compact knots are also observed in V959 Mon and, due to its high brightness temperature ($T_b \sim 2\times10^6$ K) [8], attributed to non-thermal synchrotron radiation.

The model proposed is that initially, dense, low-velocity material propelled by orbital motion drifts out along the equatorial plane of the binary (corresponding to a north–south orientation in V959 Mon), forming a more spherical geometry. This is then followed by a fast prolonged wind that propagates more easily along the low-density polar directions, creating a bipolar morphology. This would appear from east to west in the case of V959 Mon (perpendicular to the orbital plane). The material expanding along the poles dominates the radio images in the beginning, when the ejecta is optically thick. After the white dwarf wind ceases, the polar outflow will detach from the binary and quickly drop in density as it expands and becomes optically thin, leaving the slower, still optically thick, orbital driven component to dominate radio images. This model would explain V959 Mon's shift from an east–west orientation to a north–south orientation [8, 59].

Shocks are produced at the interface when these two outflows collide with one another. These shocks are most powerful near the equatorial plane where the density contrast is largest. There we observe synchrotron emission, that is also observed as synchrotron self-absorbed radio knots, and relativistic particle acceleration responsible for the observed γ rays. These shocks can be divided in a forward shock in the ejecta and a reverse shock in the nova wind, separated by a layer of cold material [7, 55]. Radio emission from the reverse shock is strongly attenuated by free-free absorption in the dense cool shell and is therefore negligible in comparison to the forward shock emission in a 1D model [7, 55]. On the other hand the reverse shocks can be important in the emission of the γ-ray.

In radio imaging of other novae, a flip of the major axis similar to the observed in V959Mon has been proposed [8]. Furthermore, a study of the spectral evolution of twelve Galactic novae reveals that they all show signs of the presence of at least two physically distinct flows [4]. These flows are consistent with the previously described ejecta's evolution and the presence of shocks. This suggests that the V959 Mon mass-loss scenario may be common in many other CNe.

γ-rays in novae were first detected in the nova V407 Cyg, where the shocks were due to the interaction between the wind of the companion red giant and the ejecta [60]. Since then, γ-rays were detected in fourteen more CNe, some of which do not have evidence of being embedded in a wind of the companion or being recurrent novae, which further supports the internal shock scenario [7, 8]. None of these novae have unusual properties which strengthens the hypothesis that all novae are γ-ray emitters but the existing γ-rays telescopes are only able to detect the nearby ones (within 4.5 kpc) [61, 62]. The differences in the detection of

γ-rays between nearby novae can also be attributed to variations in the viewing angle [6, 7].

Nevertheless, studies indicate that the γ-ray luminosities span at least two orders of magnitude so not all novae emit the same γ-ray flux [11]. So far no correlations between γ-ray luminosity and any novae properties have been found [12].

When the shocks accelerate particles to GeV energies most of the shock power is emitted through X-ray emission due to the thermal particles. However, some of that power goes to the detected γ-rays. These γ-rays can be generated in one of two potential scenarios: the leptonic or the hadronic [63, 64]. The accelerated relativistic particles that produced γ-ray emission, can very likely also produce synchrotron emission detected on the radio. This allows us to use the radio emission as a tracer of γ-ray production given that the radio lasts longer and allows for a much higher spatial resolution than the γ-rays themselves [8].

Radio observations can, in principle, help disentangle leptonic from hadronic models [7]. In the leptonic scenario, electrons that are accelerated up to relativistic speeds, emit γ-rays via *bremsstrahlung* and inverse Compton processes. These electrons also power the radio emission. In the hadronic scenario, accelerated ions that collide with a dense medium produce neutral pions, π^0, that primarily decay into a pair of γ-ray photons. Radio-emitting e^+/e^- pairs are also produced in this scenario by the decay of the charged pions, π^+ and π^-.

Various studies have focused on using shock radio emission to identify which model is the correct scenario for γ-ray generation [6, 54, 65] and most recent studies favor the hadronic scenario [66]. There are, however, strong signs that the observed radio emission is likely dominated by primary electrons directly accelerated at the shock (i.e. the radio emission is leptonic even if the γ-rays are hadronic) [66].

Chapter 2

Methods

In this chapter we will present the methods used to model the thermal emission and implement the Markov chain Monte Carlo (MCMC) method, in particular the `emcee` code. An excerpt of the code demonstrating its implementations in `Python` is presented in appendix A.

2.1 Thermal Emission Modelling

The radio emission from novae was first modelled based on a "Hubble Flow Model" implemented by [2] and described below.

We now know that novae are non-spherical [67, 68], with some of the novae studied in this dissertation showing signs of bipolar and other non-trivial geometries. Nonetheless the "Hubble Flow Model" remains a useful approximation for the behavior of the thermal radio emission in these geometries [56, 69]

As it was described in section 1.3, the "Hubble Flow Model" assumes an instantaneous ejection which implies an outer and inner hard edge in the shell (Figure 2.1). The outer and inner edges (r_2 and r_1, respectively) at time t are given by:

$$r_2 = v_{exp}t \qquad r_1 = ff\, r_2 \tag{2.1}$$

where v_{exp} represents the maximum expansion velocity and ff represents the filling factor.

Considering j_ν, the mass-emission coefficient, and k_ν, the mass-absorption coefficient, the Plank Function $B_\nu(T_e)$, which represents the spectral radiance of an object at temperature T_e as a function of frequency ν, is given by:

$$B_\nu(T_e) = j_\nu/k_\nu = (2h\nu^3/c^2)/[\exp h\nu/k_B T_e) - 1] \tag{2.2}$$

For radio frequencies the mass-emission coefficient for this type of processes can be simplified as [70, 71]:

$$j_\nu = 5.4 \times 10^{-39} N_e^2 T_e^{-1/2} g_{ff} \exp(-h\nu/k_B T_e) \tag{2.3}$$

where N_e is the electron density and g_{ff} is the Gaunt factor. For free-free emission and for $\nu < 10^{12}$ Hz, it is given by [72]:

$$g_{ff}(\nu, T_e) = (3^{1/2}/\pi)[17.7 + \log(T_e^{3/2}/\nu)] \tag{2.4}$$

Concluding, the flux density for frequency ν received by an observer on Earth is given by:

$$S_\nu = [2\pi B_\nu(T_e)/d^2] \int_0^{r_2} a[1 - \exp(-\tau_\nu(a))]da \tag{2.5}$$

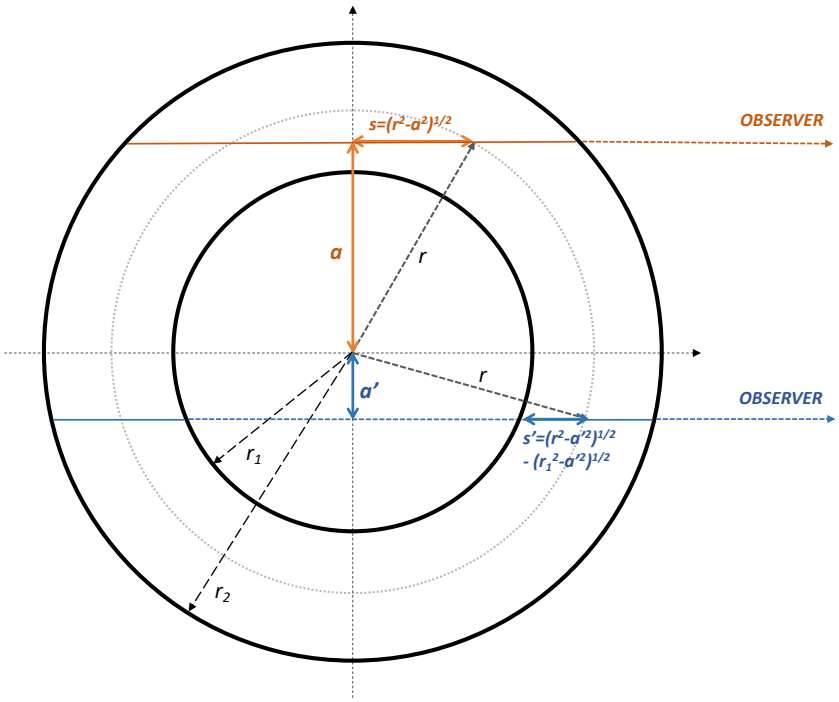

Figure 2.1: Geometry used to derive the equations for the flux density in the "Hubble Flow Model" with the lines of sight shown for the two cases. Replicated from [2].

---

where $\tau_\nu(a)$ is the optical depth at frequency ν for the line of sight corresponding to a and d is the distance to the nova for an observer on Earth.

This equation can be integrated over all possible values of a. As can be seen in Figure 2.1, we can rewrite $\tau_\nu(a)$ in terms of s:

$$\tau_\nu(a) = 2 \int_{s_1}^{s_2} k_\nu \ \rho \ ds \tag{2.6}$$

where k_ν is defined using eq. (2.2) and $s_2 = (r_2^2 - a^2)^{1/2}$, and $s_1 = 0$, if $r_1 \leq a \leq r_2$, and $s_1 = (r_1^2 - a^2)^{1/2}$, if $0 \leq a \leq r_1$.

We also use the function below that was defined in the original article and simplify it for emissions in the radio wavelength

$$F(\nu, T_e, M) = (N_e/\rho)^2 \exp(-h\nu/kT_e)[M/(4\pi)]^2[5.4 \times 10^{-39} T_e^{-1/2} g_{ff}] \tag{2.7}$$

In this work we adopt a value of 2.33×10^{-24} for ρ/N_e, the relation between the mass density ρ and the electron density. A different value for this constant translates in a scaling of the derived masses. Clumping in the ejecta (as discussed in section 1.3) will imply different values for N_e and therefore also translate in different values for the derived mass.

Finally, the equation for the optical depth becomes

$$\tau_\nu(a) = F(\nu, T_e, M)/[B_\nu(T_e)(r_2 - r_1)^2]2 \int_{s_1}^{s_2} ds/(a^2 + s^2)^2 \tag{2.8}$$

Integrating eq. (2.8) for $0 \leq a \leq r_1$ and $r_1 \leq a \leq r_2$, we can then numerically integrate eq. (2.5) and obtain the expected flux density at the Earth for each frequency.

The "Hubble Flow Model" was first published in [2] and applied on the data from three novae. To validate our implementation of the model we replicated the results for the nova HR Delphini (HR Del) using the data and derived parameters ($d = 0.8$ kpc, $v_{exp} = 450$ km s^{-1}, ff= 0.44, $M = 8.6 \times 10^{-5} M_{\odot}$, $T_e = 10^4$ K) from [2]. The resulting plot can be seen in Figure 2.2 and shows that the model replicates well the data.

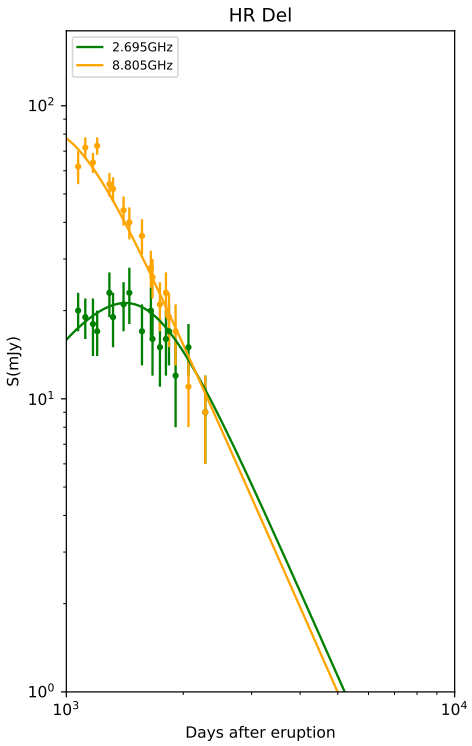

Figure 2.2: In order to validate our model implementation we replicated the results from [2]. The thermal model (solid lines) took input parameters $d = 0.8$ kpc, $v_{exp} = 450$ km s^{-1}, ff= 0.44, $M = 8.6 \times 10^{-5} M_{\odot}$, $T_e = 10^4$ K and superimposed over the VLA observations of HR Del.

2.2 Bayesian Statistics

The Bayes theorem gives the probability that a given hypothesis H is true given the data X and some background information I that we know, $p(H|X, I)$:

$$p(H|X, I) = \frac{p(X|H, I)\ p(H|I)}{p(X|I)} \tag{2.9}$$

where $p(X|H, I)$ is the posterior distribution, $p(H|I)$ is the prior distribution and $p(X|I)$ is a normalization factor called evidence.

The posterior distribution $p(X|H, I)$ represents the knowledge coming from the data, i.e. the probability that we would have observed the data given the hypothesis was true. This is expressed through the likelihood function $\mathcal{L}$. In the fitting done in this work we maximize the likelihood of our model S_{model} given the observational data S_{data}, the variance σ and a parameter f. In the simplest case $\mathcal{L}$ can be written as:

$$\mathcal{L} = \ln p(S_{model}|S_{data}, \sigma, f) = -\sum_n \left[\frac{(S_{data,n} - S_{model,n})^2}{2s_n^2} + \ln(s_n^2) \right] \tag{2.10}$$

where

$$s_n^2 = \sigma^2 + S_{model,n}^2 \exp(2 \ln(f)) \tag{2.11}$$

Equation 2.10 can be recognized as the least squares minimization however, with the added term in eq. 2.11. This assumes that the noise associated with the the observations can be considered a Gaussian process where the variance σ is underestimated by some fractional amount f, that works as a scaling factor.

The prior distribution $p(H|I)$ summarizes any prior knowledge we have about each particular parameter before we have analyzed the current data. The remaining term $p(X|I)$ is a normalizing constant dependent only on the data. This factor is more relevant for model selection, while for parameter estimation it can be neglected. Therefore, we can write the posterior distribution $p(H|X, I)$ as:

$$p(H|X, I) \propto p(X|H, I)\ p(H|I) \tag{2.12}$$

This is the general form of the equation that will be used to determine the best fit parameter in the section 2.4 using MCMC. The prior distribution will take values that are based on our knowledge (Table 3.1): if the value is within the acceptable range, the function takes a value of a normal distribution with mean 0 and a sigma value of 10, otherwise it takes a value of 0.

2.3 Outlier Detection

Some of the nova in this work show double (or more) peaks in the radio light curve, with the first peak being attributed to synchotron emission. Even in the novae where there is only one peak, there is signs that the synchotron emission also contributes to the shape and the peak flux of the radio light curve. A "Hubble Flow Model" fitting is not able to adequately distinguish the thermal component. However, assuming a different distribution of the noise helps in this identification and lowers the weight of the synchotron component.

An alternative model for the distribution of the noise was implemented in this work. The use of the Cauchy-Lorentz distribution allows us to reduce the weight of the outliers, in this case the points where the non-thermal emission is more dominant. For this distribution the likelihood function is given by:

$$\mathcal{L} = \ln p(S_{model}|S_{data}, \sigma, f) = -\sum_n \left[\ln\left(1 + \frac{(S_{data,n} - S_{model,n}))^2}{2s_n^2}\right) + \ln(s_n^2) \right] \tag{2.13}$$

with s_n^2 given by the same expression as eq. 2.11.

The effect of this alternative model can be seen on Figure 2.3. With the outlier detection method the "Hubble Flow Model" shows a better fit, compared to the simple least-squares implementation of eq. 2.10, for the second peak with a lower weight for the first peak that has a behavior badly described by a thermal model and is likely dominated by the non-thermal emission.

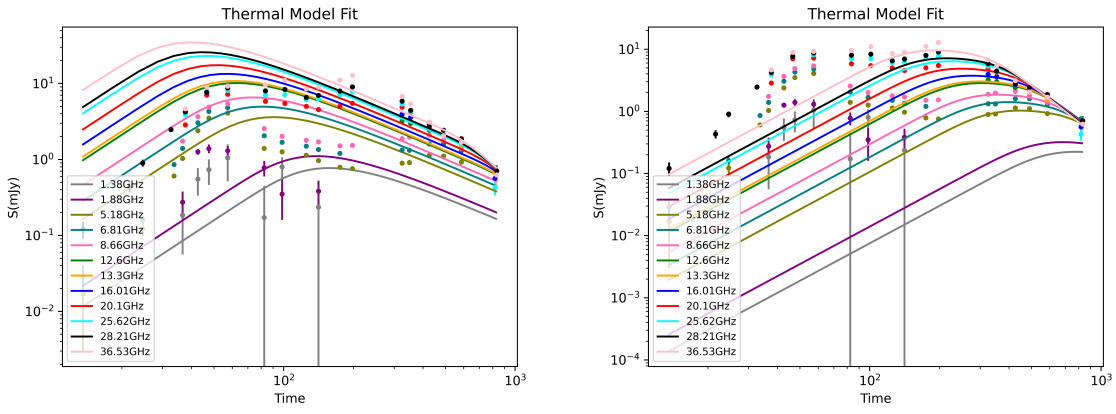

(a) (b)

Figure 2.3: Fit to the radio flux using data of nova V1723 Aql, considering all data points, *before* (left) and *after* (right) implementing an outlier detection method.

2.4 Markov Chain Monte Carlo (MCMC) method

The optimum fit for the parameters of the model was found using a MCMC method. In particular, we use the `emcee` code [13] which implements the affine-invariant ensemble sampler originally presented in [14]. In this algorithm multiple parallel MCMC chains (called walkers) are run and allowed to interact without violating the Markovian property (the choice of next step does not depend on the previous information). Because the ensemble of walkers moves in parallel, it can be parallelised in order to take advantage of a computer cluster.

In each step each walker randomly selects another walker from the ensemble and chooses a new position on the parameter space based on a random linear combination of the positions of both walkers (this is known as a stretch move). Depending on the value of the likelihood function (e.g. eq. 2.10) corresponding to the new set of parameters the step may be accepted or not (steps that increase the probability are always accepted, while steps with lower probability are sometimes rejected). This allows a more efficient exploration of the parameter space since if some walker gets near a probability maximum, it will "pull the others".

After a sufficient number of steps, the density of walkers in a region of the parameter space will reflect the value of $p(S_{model}|S_{data}, \sigma, f)$ in that region. Based on the history of walker positions we can also measure the mean and variance of each parameter.

To each parameter we choose the value corresponding to the mean of the density of values of the walkers and the uncertainties corresponding to one standard deviation above and below the mean.

Based on our preliminary simulations, the number of walkers needs not to be much higher than the dimensionality of the problem, with the convergence being much more dependent on the number of steps.

Different values of the stretch scale parameter a as defined in [14] were tested but the default value of $a = 2$ was used. The increase in the parameter allows a faster and further exploration of the space, although less detailed. It can be particularly helpful in finding local maxima of the likelihood surface, located away from the global maximum. The bigger drawback is a sharp decrease in the acceptance fraction a_f, the fraction of proposed steps that are accepted, which can be counterbalanced through the use of more steps.

Chapter 3

Results and Discussion

Seven CNe with radio observations were studied in this dissertation. The novae V959 Mon, V1324 Sco, V5668 Sgr, V357 Mus and V906 Car were detected at γ-ray wavelength while V5589 Sgr and V1723 Aql were non-detections. In the case of novae V5668 Sgr and V357 Mus these present new results while the others are have been published elsewhere.

The observed radio light curves were fit with the model curves described in the previous chapter.

The input parameters for the fit are the distance, d, the effective temperature, T_e, the maximum expansion velocity v_{exp}, the filling factor *ff*, the ejecta mass M_{ej} and the scalling factor f. The free parameters are actually degenerate - multiple combinations of parameters produce very similar radio light curves: an increase in distance results in a higher maximum flux density; an increase in temperature results in an earlier turnover from optically thick to thin and a higher flux at all times; an increase in maximum velocity also results in an earlier turnover; an increase in the filling factor results in a thicker ejecta which lowers the maximum flux density and slows the decline after the peak and an increase in ejecta mass results in a a higher flux at all times and delays and slows down the turnover [48].

Since the electron temperature T_e is degenerate with other parameters and its value for CNe has only small fluctuations around 10^4K, this parameter was fixed at the value of $T_e = 10^4K$. Of the remaining 5 parameters, the distance to the nova is the most readily available in the literature. Therefore, the fitting was performed with only v_{exp}, *ff*, M_{ej} and f as free parameters. All frequencies were fit at the same time.

The ejection time is assumed to be coincidental with the detection of the nova on the optical wavelengths, unless otherwise stated. Multiple studies indicate that certain novae have delayed ejections [56, 58], which may produce shocks.

The MCMC walkers were initialized with a gaussian distribution around previously chosen values for each nova. For the scalling factor f the value choosen is 1 for all novae. The values of the remaining parameters were chosen based on the values obtained in the published literature. In the cases of unpublished observations, values were chosen based on possible ranges (see priors in Table 3.1). One hundred walkers were initialized and 10^5 steps, in order to fully sample the parameter space. The first 100 steps were discarded as burn-in.

Table 3.1: Value ranges of acceptable priors based on physical limits of known nova parameters.

$\log(v_{exp})$	[2.0, 4.1]
ff	[0.0, 1.0]
$\log(M_{ej})$	[-7.0, -2.0]
$\log(f)$	[-10.0, 1.0]

The priors were bound, between physically acceptable values in a nova eruption (Table 3.1), such that if the value on the parameter space of a given step is outside of that limit

range, the associated probability is null.

In section 3.1 the individual novae are discussed and the derived best fit parameters presented in Table 3.2. In Figures 3.1-3.8 the observed fluxes and best fit thermal model, brightness temperature, residuals, and spectral indexes are presented.

The individual nova brightness temperature was calculated using eq. (1.3) with the velocity of the ejecta being given by the best fit parameter. The horizontal dashed line on the plots represents $T_b = 5 \times 10^4$, the highest temperature that we consider can be expected from thermal emission alone.

Some of the novae studied in this work show brightness temperatures at early times ($t < 100$ days) higher than that expected for thermal emission alone. At later times, as expected from thermal emission, when the ejecta transitions into being optically thin and emission from the interior of the ejecta is observed, the derived temperatures are lower than 10^4 K.

There are two clues that the measured T_b are likely lower limits to the true T_b. 1) High-resolution imaging has shown synchrotron emission is often arranged as compact knots on top of a more diffuse thermal ejecta [8], therefore lowering the predicted T_b. And, 2) the fact that the ejecta is, more often than not, non-spherical and not homogenous, will also set a lower limit to the T_b values derived [56].

The spectral index, α, was calculated for each date with more than two frequencies. The values were obtained through a linear regression in log space using the function `polyfit` from the package `numpy` with the corresponding error obtained from the covariance matrix. We did the calculations considering only the low frequencies, the high frequencies and both [1].

The residual plots are the arithmetic subtraction of the observed and model fluxes and make the assumption that the residual flux is due to non-thermal emission. The spectral indexes of the residuals are also shown.

In Table 3.2 the γ-ray fluxes, either as detections or upper limits, along with, when relevant, their duration and their associated γ-ray luminosities are presented. These luminosities or luminosity upper limits, L, were calculated using:

$$L = 4\pi d^2 F \tag{3.1}$$

where F is γ-ray flux or the flux upper limit and d is the distance to the nova.

All the radio data was obtained from the Karl G. Jansky Very Large Array (VLA) [73], in Socorro, New Mexico, with the exception of the data from V357 Mus and V906 Car that was obtained from the Australia Telescope Compact Array (ATCA), Paul Wild Observatory, Australia [74]. The VLA comprises of 28 (27 active and 1 spare) 25-meter-diameter parabolic dishes arrayed in a Y-shaped configuration that allows them to function as an interferometer and be electronically combined to provide the resolution of an antenna 36 kilometers wide. It samples the frequency range from 1.0 GHz to 50 GHz. The ATCA comprises of six 22-meter-diameter parabolic dishes, which can simulate a single dish with a diameter of 6 kilometers. It is the only telescope of its sort in the Southern Hemisphere, operating in the frequency range 1.1 GHz to 105 GHz.

All the γ-ray data was obtained by the Fermi Large Area Telescope (LAT) [75]. This is the main instrument onboard the Fermi Gamma Ray Space Telescope spacecraft, that orbits in a low-Earth circular orbit. LAT is a high-energy imaging γ-ray telescope with a range of energy from roughly 20 MeV to more than 300 GeV. At any given time, its field of view covers about 20% of the sky, and it scans continually, covering the entire sky every three hours.

[1] Through out the work frequencies below 10 GHz are refereed to as *low frequencies*, as opposed to the *high frequencies*.

Table 3.2: Detailed nova information based on previously published data and derived parameters from the MCMC fits.

	Date Range	Radio Flux Ref	Distance (kpc)	v_{exp} (km/s)	ff	$\ln(f)$	M_{ej} ($M_\odot$)	γ-ray Flux ($10^{-7} cm^{-2} s^{-1}$)	Duration (days)	γ-ray Luminosity (photons s^{-1})
Novae with γ-ray emission										
V959 Mon	2012 Jun 30–2014 Feb 25	[8]	1.4 ± 0.4 [76]	2624^{+171}_{-108}	$0.106^{+0.010}_{-0.013}$	$-7.58^{+1.60}_{-1.59}$	$\left(12.9^{+0.6}_{-0.8}\right) \times 10^{-5}$	5.2 ±0.5 [11]	22 [11]	$(1.22 \pm 0.12) \times 10^{38}$
V1324 Sco	2012 Jun 26–2014 Dec 18	[57]	4.3 ±0.9 [77]	607^{+49}_{-35}	$0.563^{+0.290}_{-0.196}$	$-6.48^{+2.08}_{-2.28}$	$\left(3.1^{+4.4}_{-1.1}\right) \times 10^{-5}$	5.0 ±0.5 [11]	17 [11]	$(1.11 \pm 0.11) \times 10^{39}$
V5668 Sgr	2015 Mar 17–2019 Dec 22	[78]	2.8 ± 0.5 [79]	1783^{+113}_{-171}	$0.307^{+0.677}_{-0.048}$	$-7.05^{+1.89}_{-1.91}$	$\left(57.6^{+2.6}_{-43.2}\right) \times 10^{-5}$	0.8 ±0.1 [11]	55 [11]	$(3.83 \pm 0.48) \times 10^{37}$
V357 Mus	2018 Jan 18–2020 Sep 12	[78]	$3.3^{+1.2}_{-0.7}$ [78]	1195^{+52}_{-47}	$0.172^{+0.045}_{-0.043}$	$-6.61^{+2.03}_{-2.20}$	$\left(14.7^{+0.8}_{-0.7}\right) \times 10^{-5}$	1.3 ± 0.2 [79]	27 [79]	$(1.69 \pm 0.26) \times 10^{38}$
V906 Car	2018 Apr 3–2020 Sep 12	[58, 78]	4.0 ±1.5 [58]	1611^{+45}_{-44}	$0.203^{+0.456}_{-0.141}$	$-6.50^{+2.16}_{-2.26}$	$\left(106.1^{+19.9}_{-52.1}\right) \times 10^{-5}$	12.2 ±0.4 [79]	23 [79] [2]	$(2.34 \pm 0.75) \times 10^{39}$
Novae without γ-ray emission										
V5589 Sgr	2012 Apr 23–2013 Aug 26	[56]	$7.7^{+5.2}_{-3.2}$ [48]	4×10^3 [48]	$0.801^{+0.121}_{-0.125}$	$-6.29^{+2.26}_{-2.40}$	$\left(42.6^{+0.7}_{-1.2}\right) \times 10^{-5}$	< 1.3 [11]		$< 9.22 \times 10^{38}$
V1723 Aql	2010 Sep 25–2014 Mar 15	[48, 80]	5.7 ±0.4 [48]	2259^{+87}_{-221}	$0.073^{+0.010}_{-0.008}$	$-7.36^{+1.70}_{-1.74}$	$\left(22.8^{+0.9}_{-2.0}\right) \times 10^{-5}$	< 2.3 [11]		$< 8.94 \times 10^{38}$

[2]The start time of γ-ray detection for V906 Car was not captured due to Fermi-LAT downtime, and the end time is only bound to be within a date range. The γ-ray flux is calculated over the smallest data range possible.

3.1 Radio Fit Results

3.1.1 V959 Mon

Due to its solar conjunction, nova V959 Mon (Nova Mon 2012) was first detected in γ-rays beginning on June 22 2012 [81] with the identification as a nova and the first optical observations happening only months after the outburst. The value used for the distance in this work, $d = 1.4 \pm 0.4$ kpc was derived using a combination of radio expansion measurements from the VLA and velocities derived from optical spectra [76].

In addition to the radio flux measurements, Very-Long-Baseline Interferometry (VLBI) images at multiple epochs were also obtained which revealed a complex ejecta morphology, starting with a east to west bipolar structure detected at day 126 and evolving into a north–south structure detected at day 615 [8]. More information about the morphology of this nova can be found in section 1.4 where internal shocks were discussed.

Unlike some of the other novae on this work, there is no sign of dust formation in V959 Mon [82].

As can be seen in panel a) of Figure 3.1 the prediction of the model is a better fit at later times for high frequencies, when the expected behavior is more consistent with the optically thin thermal ejecta. At early times (t<100 days), our model is not a good fit and provides an overestimation on the flux (see panel d) on Figure 3.1). Around day 200 a first peak on low frequencies is very clear on the main plot (panel a)), becoming clear in the residuals plots that every frequency has an excess emission compared to the thermal model (panel d)).

The observed brightness temperatures are above what expected from a thermal ejecta at very early times (t<20 days) but remain below $T_B = 5 \times 10^4$ K during the rest of the evolution, albeit higher in the lower frequencies (see panel b)).

In those early times there are very few points to make a statistically significant conclusion about alpha. Around day 74 when detection on all frequencies begin, the spectral index reaches on all frequencies $\alpha = 1.79$, close to the expected for optically thick emission ($\alpha = 2$). It has a soft decay after that, with the high frequencies decaying first as expected (see panel c)).

Previous fittings of the late time (t>200 days) radio data with an "Hubble Flow" model, derive an ejecta mass of $M_{ej} = 0.4 \times 10^{-4} M_\odot$ and an electron temperature of $T_e = 2 \times 10^4$ K, keeping fixed the distance at $d = 1.5$ kpc, and the maximum expansion velocity at $v_{exp} = 2400$km s^{-1} [8].

On our fit we fix the distance at $d = 1.4$ kpc, which is close to the value used on the previous fit, and the electron temperature at $T_e = 10^4$ K, which is half of the one derived on the previous fit. Our derived maximum expansion velocity, $v_{exp} = 2624^{+171}_{-108}$ kms^{-1} is close to the one used on the previous fit and our derived ejecta mass, $M_{ej} = \left(1.29^{+0.06}_{-0.08}\right) \times 10^{-4} M_\odot$ is just a factor of $\sim$3 bigger.

3.1.2 V1324 Sco

V1324 Sco (Nova Scorpii 2012) was discovered on May 22 2012 at optical wavelengths [83] and began emitting γ rays 15 days after the outburst [57]. This nova was the second CN observed in γ-rays. Out of the 7 analised in this work, this is the most luminous on the γ-ray band and is the farthest with detected γ-ray emission.

The value used for the distance in this work, $d = 4 \pm 1.5$ kpc was derived using the novae reddening and the Galactic reddening–distance relation [77]. However, other studies using high-resolution optical spectroscopy find a distance limit of $d > 6.5$ kpc [84]. This higher

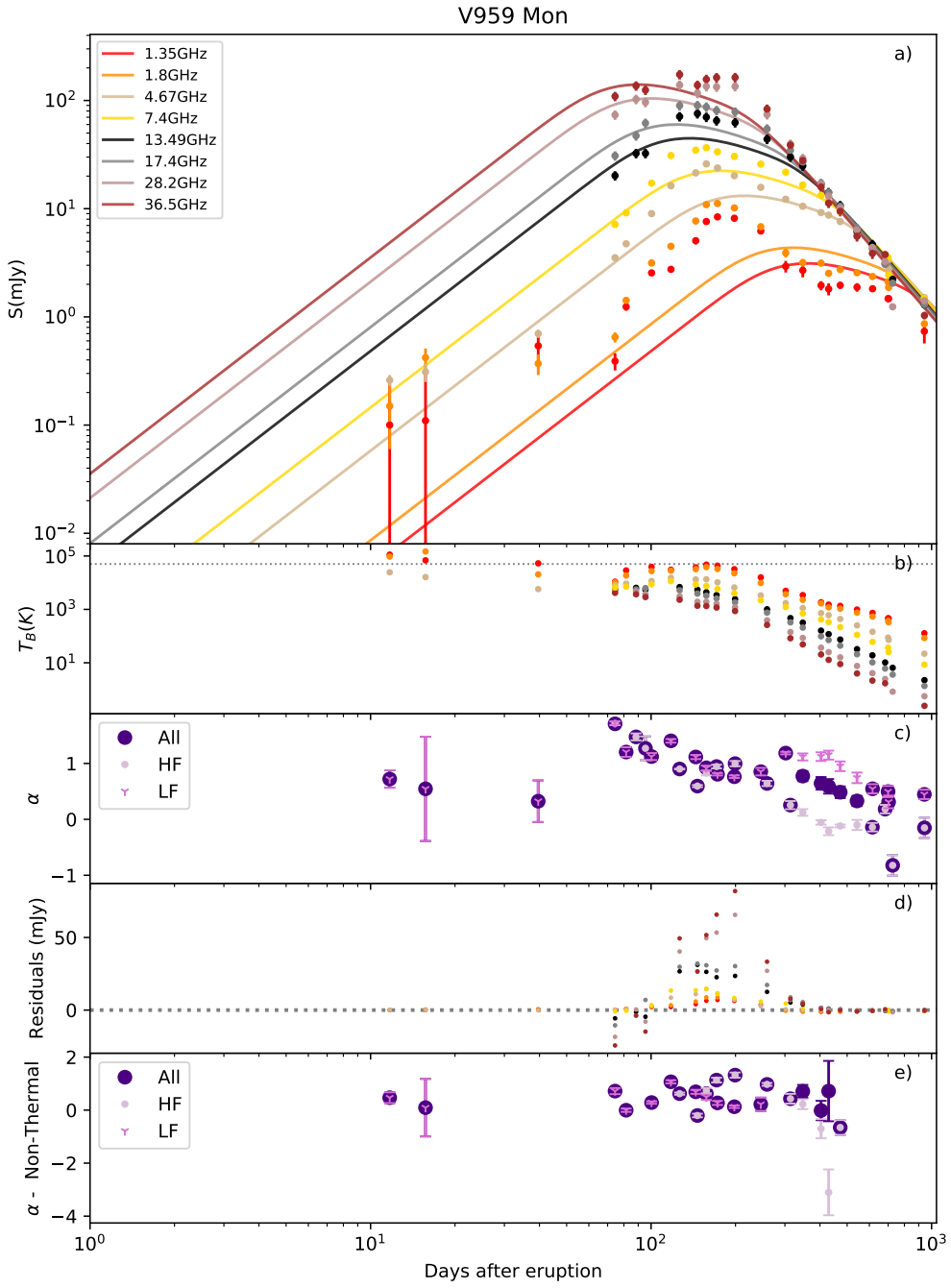

Figure 3.1: Results for the fit of the thermal model on the nova V959Mon. Panel a) Observed fluxes (round symbols) and the thermal model fit (solid lines). Panel b) The brightness temperature. Panel c) The spectral index α calculated for each time value that had data points corresponding to more than two frequencies. Panel d) Residual flux, resulting from the subtraction of the observations and model. Panel e) Spectral index of the residual plot.

distance value shifts not only the predicted thermal radio curve up but also increases the predicted γ-ray luminosity.

Such as the previously discussed nova, V1324 Sco presents a double-peaked radio light curve, with the first peak happening on day $\sim$70 and the second peak $\sim$1 year after eruption, with the high frequencies peaking first. The second peak has a behavior consistent with thermal emission from the expanding nova ejecta and shows a much better fit with our model (panel a) of Figure 3.2), albeit producing an over prevision before the decay of the second peak ($t \sim 200$ days). The first radio detection at day +25 was only observed on two frequencies, so the possibility of an additional peak happening before the peak that happens at +72 cannot be excluded.

Around the early peak the eruption shows high brightness temperatures at low frequencies (see panel b)), higher than what could be explained by thermal emission alone and a clear peak can be observed on the residuals plot (see panel d)).

The predicted $\alpha = 2$ during the rise is never reached but we observe an increase in the spectral index reaching $\alpha = 1.5 \pm 0.47$ for high frequencies at day 164 before decreasing again when the ejecta becomes optically thin (see panel c)),. The spectrum flattens first at higher frequencies as expected from the model.

During the initial rise $S \propto t^{2.9}$ [57], which is more consistent with non-thermal emission and not the expected for thermal $S \propto t^2$. The rise to the second maximum is consistent with the thermal emission, with the rise at 7.8 GHz having a power-law index of 2, while the rise at 17.5 GHz has a power-law index of 1.7, with the variation being attributed to a higher weight of the non-thermal component in the higher frequency during the rise to the second peak [57].

We can observe at late times (see panel a)) that, as predicted by a negative spectral index, the tendency inverts and higher frequencies start having lower emissions than the lower frequencies.

V1324 Sco produced an exceptionally dramatic dust event in comparison to previous novae. Despite this, the expected X-ray emission associated with these events was not observed [57].

Previous fittings of just the second bump (t>106 days) radio data with the Hubble flow, derive an ejecta mass of $M_{ej} = (1.4 \pm 0.5) \times 10^{-4} M_\odot$ and a distance of $d = 14.8 \pm 1.6$ kpc, having kept fixed the electron temperature at $T_e = 10^4$ K and the maximum expansion velocity at $v_{exp} = 2600 \pm 260$km s^{-1} [57]. In the article further studies are made considering the degeneracy between the parameters. Fixing the distance at $d = 6.5$ kpc, the minimum possible distance found using high-resolution optical spectroscopy [84], and the maximum expansion velocity at $v_{exp} = 1150$km s^{-1}, which is consistent with the velocity measured through the absorption curves, and maintaining $T_e = 10^4$ K, the predicted ejecta mass is $M_{ej} = (1.8 \pm 0.6) \times 10^{-5} M_\odot$.

On our fit we fix the distance at $d = 4.3$ kpc and the electron temperature at $T_e = 10^4$ K. Our derived ejecta mass is $M_{ej} = \left(3.1^{+4.4}_{-1.1}\right) \times 10^{-5} M_\odot$ and the maximum expansion velocity is $v_{exp} = 607^{+49}_{-35}$ kms^{-1}. Our value for the ejecta mass is more consistent with the predicted using a smaller distance and velocity which is expected.

The derived velocity value, in this work, lower than the measured through the absorption curves could be explained by the fact that we did not consider a delayed ejection. A later ejection would create the bigger ejecta (higher radius) required during the optically thick phase, resulting in the the predicted higher velocity.

We also did a fit constraining the velocity to $v_{exp} > 1000$km s^{-1}, maintaining the same fixed parameters. We found a derived ejecta mass of $M_{ej} = \left(5.4^{+0.3}_{-0.8}\right) \times 10^{-5} M_\odot$ and a

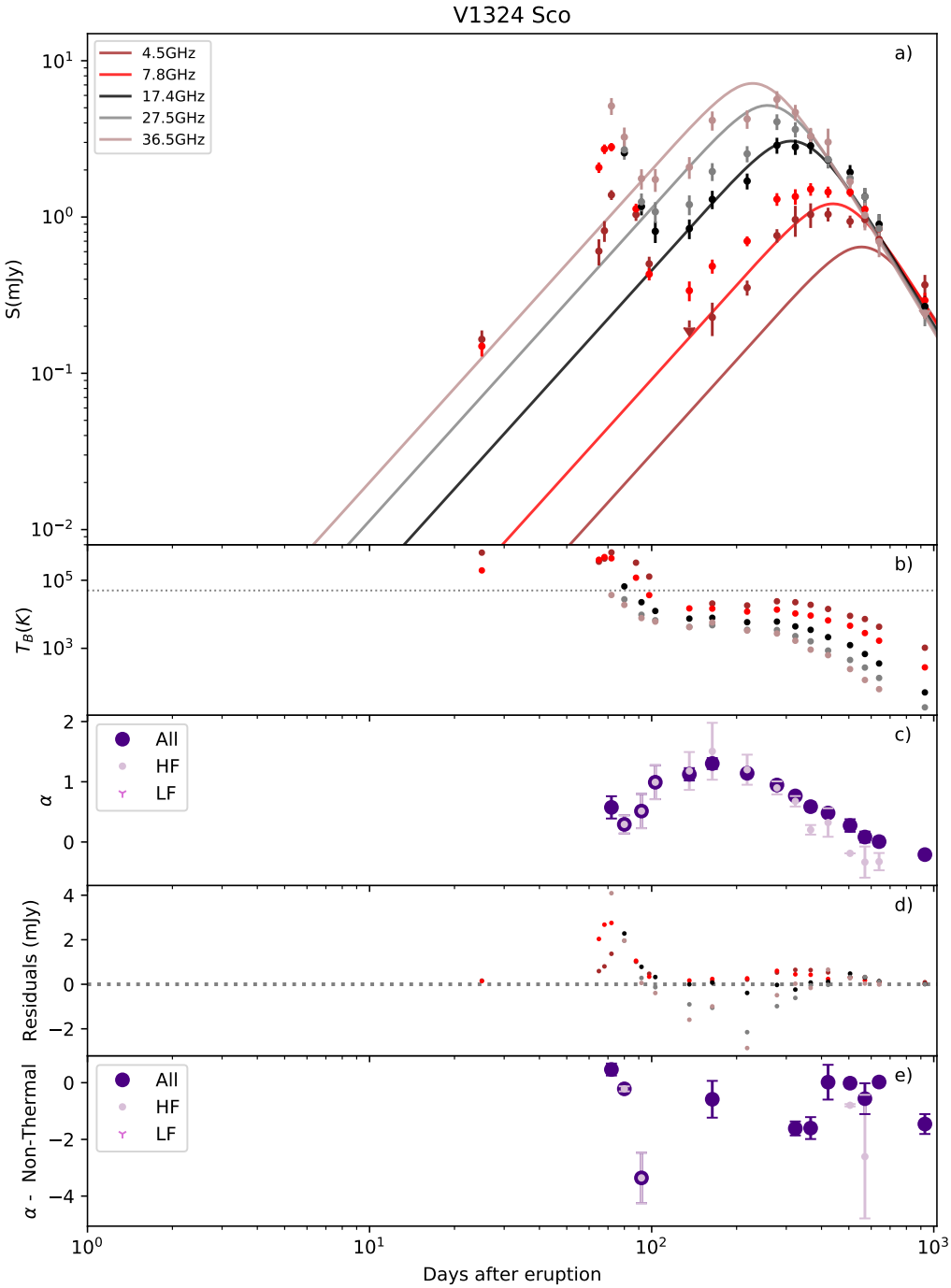

Figure 3.2: As Figure 3.1 but for V1324 Sco

maximum expansion velocity of $v_{exp} = 1007^{+18}_{-902}$ kms^{-1}. While this value of v_{exp} is more consistent with the one measured through the absorption curves, the minimum error bar is considerable. In addition, the curve provides a much worse fit to the observational data.

3.1.3 V5668 Sgr

The nova V5668 Sgr (Nova Sagittarii 2015 #2) was discovered by John Seach on March 15 2015 [85]. There were no significant γ-ray detections until $\sim$ 1.5 days following the optical peak [86]. The value used for the distance, $3.3^{+1.2}_{-0.7}$ kpc was obtained using optical spectroscopy [79].

The significant overproduction of Beryllium (^{7}Be) on this nova is particularly interesting, with some researchers suggesting that CNe may be the source of all the lithium (^{7}Li) in our galaxy [87, 88].

The brightness temperatures near the peak are high despite not reaching $T_B > 5 \times 10^4$ K (see panel b) on Figure 3.3) which does not exclude that some non-thermal mechanism has contributed to the radio emission. Unlike the 2 double peaked novae discussed before (V959 Mon and V1324 Sco), in the V5668 Sgr the thermal and non-thermal emission seem to "blend" together in a single peak in the radio light curve. We can observe on panel a) and d) that our thermal model under predicts the experimental points, and a non-thermal peak seems to emerge around day 300.

For later times ($t > 100$) the spectral index at higher frequencies decays faster than the lower frequencies (panel c)). This is consistent with the lower frequencies having a contribution from non-thermal emission for a longer time, becoming optically thin later.

The shape of the optical spectral line profiles [89] and the VLA images [90] are strong indicatives of a bipolar morphology, very similar to that observed in V959 Mon.

Simultaneous hard X-ray and γ-ray were detected in this nova [91]. There was also a link discovered between γ-ray emission and optical emission, with γ- rays detected only during epochs of increase in the brightness of the optical emission [64, 92], implying a similar source of origin, the most likely of which being internal shocks. This simultaneous emission indicates that the majority of the nova's optical luminosity was powered by shocks. A similar analysis is done for the nova V906 Car in [58]. During its optical evolution V5668 Sgr shows multiple drops in the brightness attributed to dust emission [12]. This behavior normally comes associated with double-peaked radio light curves, which is not the case here [78].

With the distance fixed at $d = 2.8$ kpc and the electron temperature at $T_e = 10^4$ K, our derived ejecta mass is $M_{ej} = \left(57.6^{+2.6}_{-43.2}\right) \times 10^{-5} M_\odot$ and the maximum expansion velocity is $v_{exp} = 1783^{+113}_{-171}$ kms^{-1}.

3.1.4 V357 Mus

The nova V357 Mus (Nova Muscae 2018) was discovered in the optical channel on January 14 2018 [93] and detected in γ-rays eight days later [94] with the radio flux measurements starting 4 days after discovery. The value used for the distance, $3.3^{+1.2}_{-0.7}$ kpc was obtained from a Gaia parallax measurement [78].

V357 Mus shows a double peaked radio light curve, with the first peak on day 64 being an order of magnitude brighter than the later peak that happens around day 594 for all frequencies except 9.0GHz (see panel a) on Figure 3.4). Our fit adheres well to the observed data for the second peak at high frequencies but, as expected, fails to predict the first peak. This early peak shows signs of a non-thermal emission mechanism from the very high brightness temperatures observed in all frequencies (see panel b) and d)). This non-thermal peak is correlated with a dust dip in the optical light curve [78].

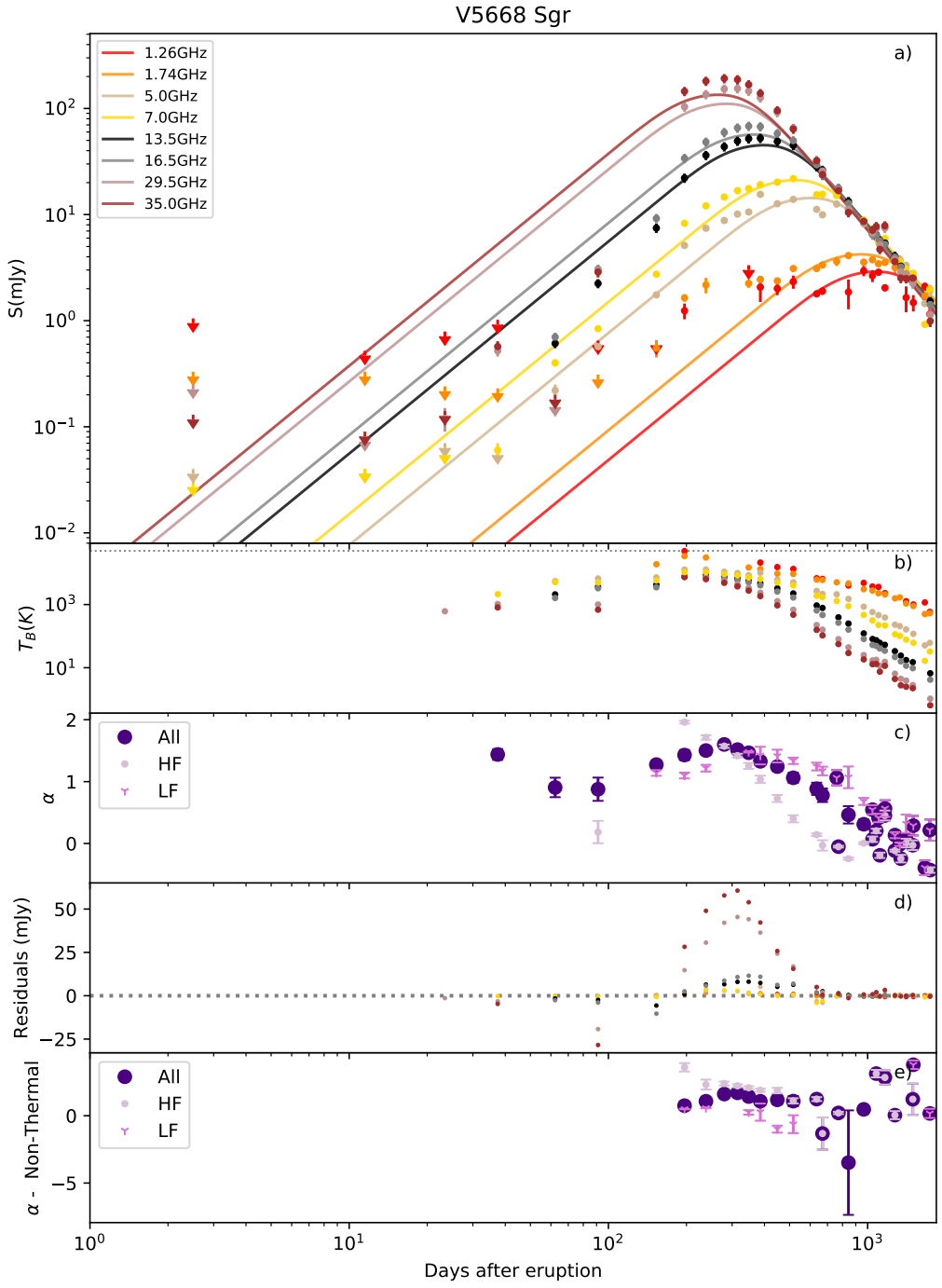

Figure 3.3: As Figure 3.1 but for V5668 Sgr

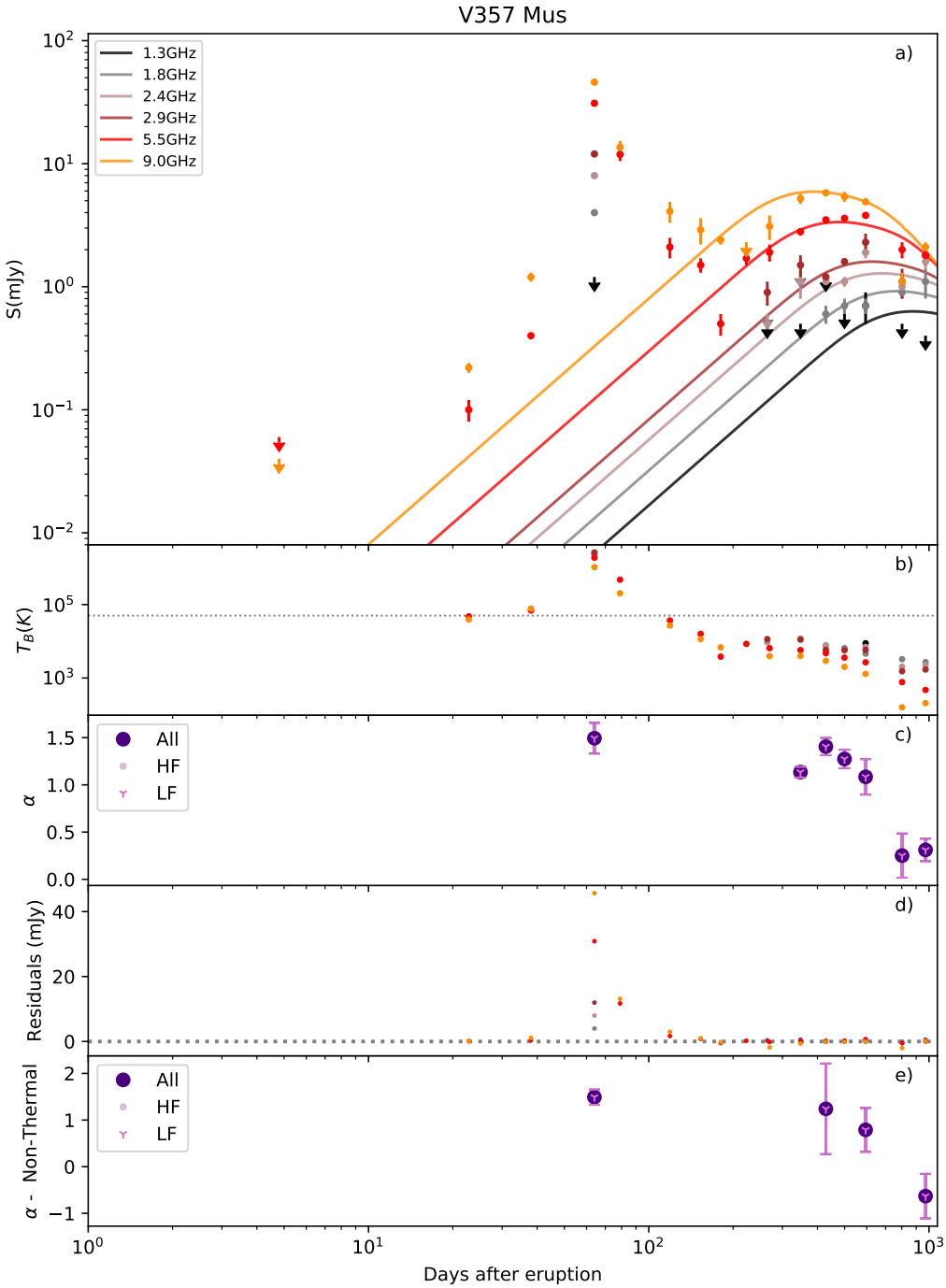

Figure 3.4: As Figure 3.1 but for V357 Mus

We do not have enough data points to extract any meaningful information about the spectral index of the total emission of the non-thermal emission (panel c) and e)), with the last points points having a big error bar and being attributed to times where the radio behavior is of optically thin thermal emission and the predicted non-thermal emission is almost negligible.

With the distance fixed at $d = 3.3$ kpc and the electron temperature at $T_e = 10^4$ K, our derived ejecta mass is $M_{ej} = \left(14.7^{+0.8}_{-0.7}\right) \times 10^{-5} M_\odot$ and the maximum expansion velocity is $v_{exp} = 1195^{+52}_{-47}$ kms^{-1}.

3.1.5 V906 Car

V906 Car (Nova Carinae 2018) was discovered in the optical channel on March 16 2018 [95]. 18 days later, the Australia Telescope Compact Array (ATCA) communicated a non-detection at radio wavelengths. The first radio detection occurred on 2018 May 13, 58 days after optical detection and $\sim$ 10 days after the last Fermi LAT detection [58].

The radio light curve continues to evolve up until present day but seems to have already reached its peak. The value used for the distance, 4 ± 1.5 kpc was obtained from Galactic reddening maps and is in good agreement with the Gaia measurements [58].

A visual analysis of the fit of the radio light curve seems to indicate a later ejection of the ejecta (or part of it). Closer studies show that a delayed expansion ($\sim$ 10–20 days after eruption) of the bulk of the ejecta is a better fit for the radio curve of V906 Car [58]. For that reason we performed two fittings of the radio light curve: one assuming a ejection coincident with day 0 (Figure 3.5) and the fit was assuming a delayed ejection of 15 days (Figure 3.6). The values used for the analysis and presented on Table (3.2) are the ones obtained with the delayed ejection. Without the delayed ejection the best fit parameters for the ejecta mass and maximum velocity are $M_{ej} = \left(103.2^{+21.1}_{-54.2}\right) \times 10^{-5} M_\odot$ and $v_{exp} = 1549^{+40}_{-37}$ km s^{-1}. The introduction of the delayed ejection resulted in a slightly higher mass and velocity ($M_{ej} = \left(106.1^{+19.9}_{-52.1}\right) \times 10^{-5} M_\odot$ and $v_{exp} = 1611^{+45}_{-44}$ km s^{-1}).

Despite not having double peaks in all frequencies, there is an excess of radio emission at early times (between days 50 and 100) compared to the Hubble Flow fit (see panel a) on Figure 3.6). Additionally, our model does not provide an adequate fit for the late times, overpredicting the emission at high frequencies (panel d)). The brightness temperatures never exceed the threshold of $T_B = 5 \times 10^4$ K (panel b)). We do not have enough data points to draw any conclusions about the evolution of the spectral index (panels c) and e)).

Simultaneous oscillations in the optical and γ-ray emissions are also found in this nova, with a twofold increase in the luminosity of the nova during the γ-ray flares, which suggests that they are caused by the same underlying mechanism - internal shocks [58]. These oscillations on the optical curve are attributed to dust formation which indicates a link between dust formation and internal shocks. An added sign of internal shocks on this nova is the attenuation of X-rays [96]. At high intensities of shocks, the resulting thermal X-rays from the heated material are attenuated or reprocessed into optical and infrared light [58].

Previous fits in the literature of the radio light curve with an "Hubble Flow" model assume that the ejection started on day 22 with an maximum expansion velocity of $v_{exp} = 2500$km s^{-1} and an electron temperature of $T_e = 10^4$ K [58]. They conclude that for the light curve to not over-predict the radio fluxes and remain optically thick for at least 533 days at frequencies as high as 9 GHz, the distance must be $d \sim 6.2$ kpc and the ejecta mass must be $M_{ej} \gtrsim 2 \times 10^{-4} M_\odot$.

If instead the ejecta started expanding on day 11 with an maximum expansion velocity of

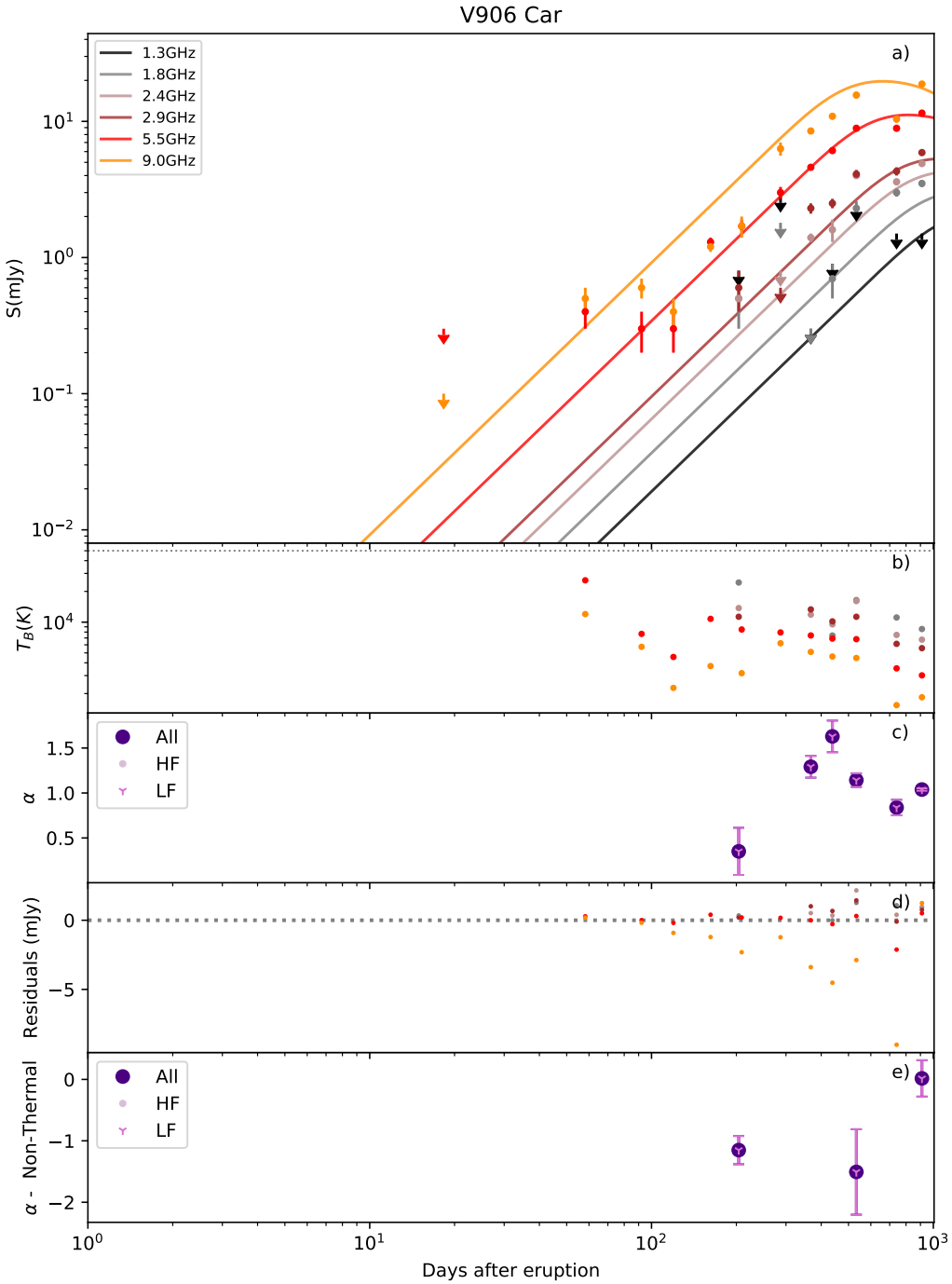

Figure 3.5: As Figure 3.1 but for V906 Car

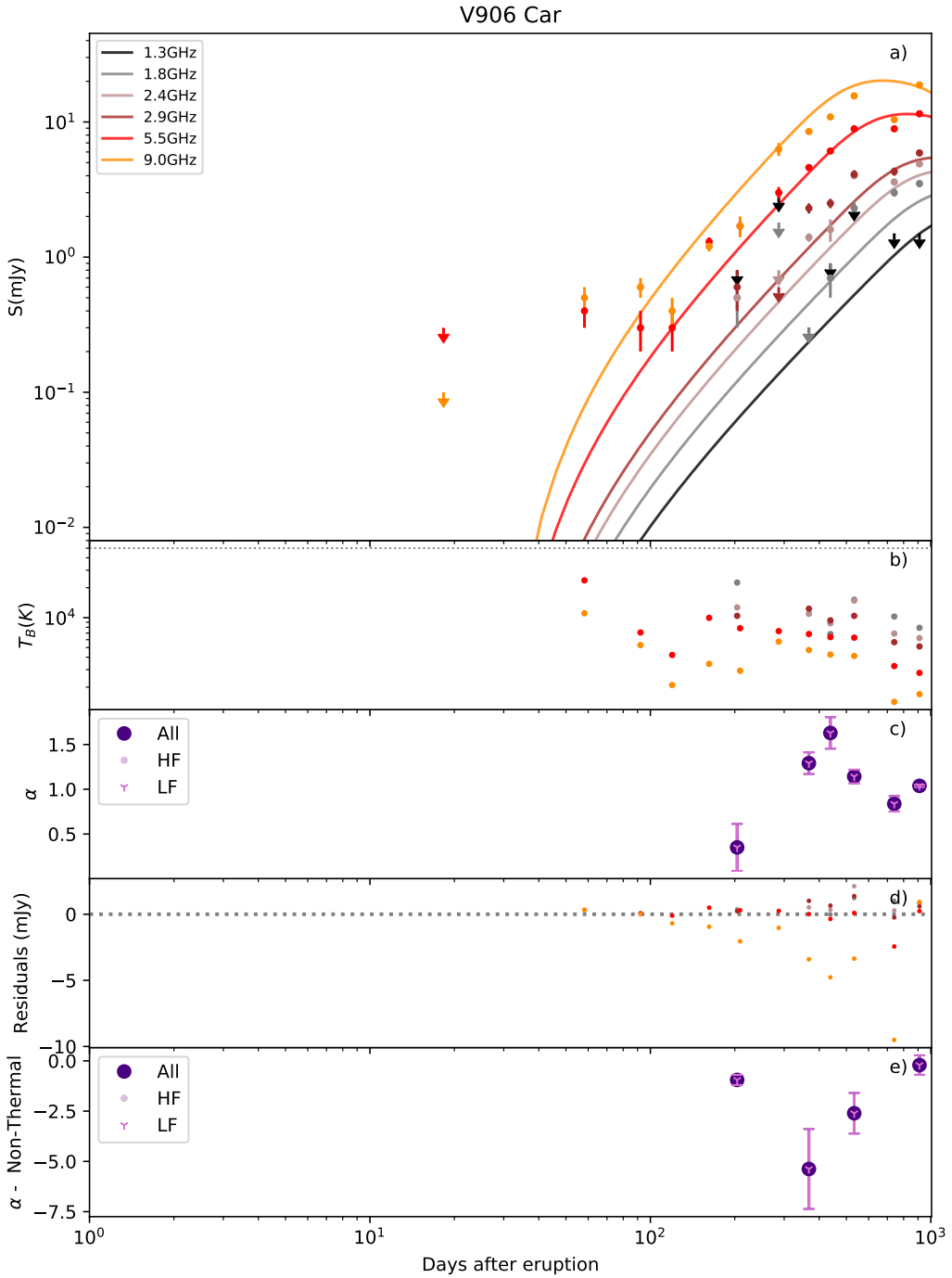

Figure 3.6: As Figure 3.1 but for V906 Car, with a delayed ejection of 15 days

$v_{exp} = 1200$km s^{-1} and maintaining the electron temperature of $T_e = 10^4$ K, the prediction is of $d = 3.4$ kpc and $M_{ej} \gtrsim 1.5 \times 10^{-4} M_\odot$. If the ejecta started expanding with the slowest velocity predicted $v_{exp} = 600$km s^{-1}, the derived parameters are $d = 1.8$ kpc and $M_{ej} \gtrsim 9 \times 10^{-5} M_\odot$.

On our fit we fix the distance at $d = 4.0$ kpc and the electron temperature at $T_e = 10^4$ K and consider a delayed ejection of 15 days. Our derived ejecta mass, $M_{ej} = \left(10.61^{+1.99}_{-5.21}\right) \times 10^{-4} M_\odot$, is consistent with the lower limits proposed by their fit. The maximum expansion velocity, $v_{exp} = 1611^{+45}_{-44}$ kms^{-1} is also consistent with the maximum value used for the earlier ejection.

3.1.6 V5589 Sgr

V5589 Sgr (Nova Sgr 2012) was first detected on optical on April 21 2012 [97]. The radio observations started three days after [56]. No signs of γ-ray were detected.

Based on the first radio non-detection and the optical spectra, the beginning of the thermal radio emission must have been between the beginning of optical detection (day 0) and day 2 [56]. Our simulations of the variation within that interval of the date of ejection of radio material produced only small variations (on the order of 10^{-2}, within the error margin) on the values of the free parameters. The value used for the distance, $7.7^{+5.2}_{-3.2}$ kpc was obtained from a Gaia parallax measurement. Based on the results of the preliminary simulations, we also fixed the value of the maximum expansion velocity at $v_{exp} = 4000$ km s^{-1} to provide a more adequate fit.

Instead of what is expected for thermal emission, the radio light curve shows a flattening as the radio flux rise with a fast increase in radio emission at low frequencies (see panel a) and c) on Figure 3.7). The initial rise, between days 46.4 and 62.3, is steeper than expected from a freely expanding source, with $S \propto t^{3.9 \pm 0.1}$ at 5.0 GHz and $S \propto t^{3.3 \pm 0.1}$ at 6.8 GHz [56]. During this rise, the spectrum flattens, with $\alpha = 0.093 \pm 0.005$ at day 54.2, the day corresponding with the maximum of the radio flux, which indicates a non-thermal origin. After that point the spectrum remains roughly flat with an outlier at day 136.20.

Other hints that this emission was powered by shocks are signs of linear polarization [56], the presence of unusually hard X-rays [56] and its high brightness temperature at early times (see panel b)). However, no signs of dust formation have been found in this nova.

As in the previously described nova V5668 (section 3.1.3), this nova only has one peak with the possibility of a second peak being excluded [78]. The high brightness temperature, above what expected from thermal emission, around that single peak is indicative of a contribution of synchrotron emission to its flux. The origin of the synchroton emission is still up for debate with internal shocks or shocks arising from the wind of a secondary star not being ruled out [78]. Determining the nature of the secondary star will be crucial to disentangle this.

Previous fittings of the entire radio light curve with an "Hubble Flow" model, derive an an ejecta mass of $M_{ej} = 2.6 \times 10^{-5} M_\odot$ and an electron temperature of $T_e = 1.2 \times 10^4$ K, keeping fixed the distance at $d = 4$ kpc and the maximum expansion velocity at $v_{exp} = 4000$km s^{-1}. This best fit is only consistent with the data during the late time (t > 100 days) and at high frequencies [56].

On our fit we fix the distance at $d = 7.7$ kpc, which is higher than the one chosen by the previous authors based on absorption features in the optical spectrum and the peak optical brightness. We also fixed the electron temperature at $T_e = 10^4$ K, which is close to the one derived on the previous fit, and the maximum expansion velocity at $v_{exp} = 4000$km s^{-1}, which we chose based on their result. However, our derived ejecta mass, $M_{ej} = \left(4.26^{+0.07}_{-0.12}\right) \times$

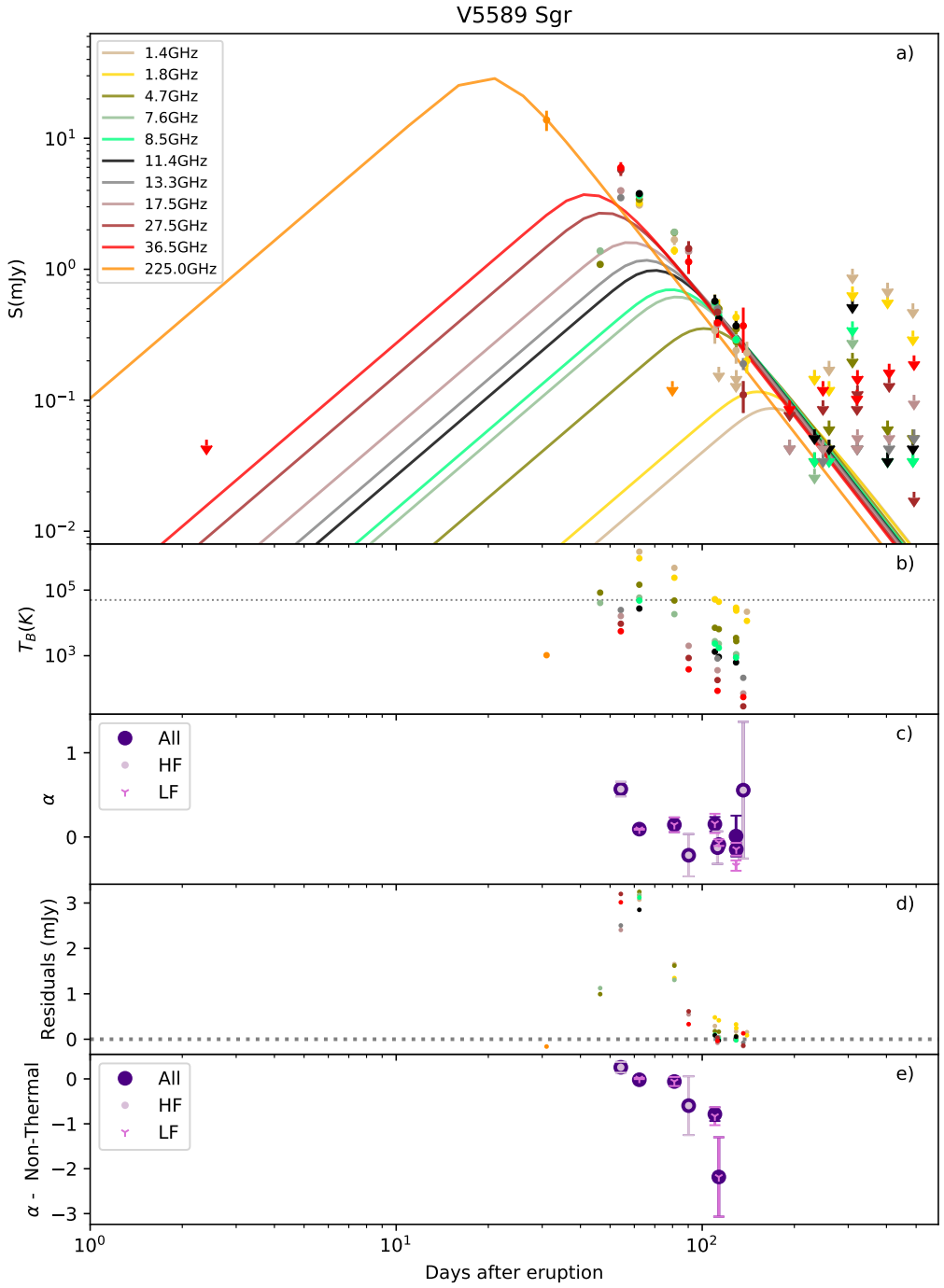

Figure 3.7: As Figure 3.1 but for V5589 Sgr

$10^{-4}M_{\odot}$ is much bigger than the one derived before.

3.1.7 V1723 Aql

V1723 Aql (Nova Aql 2010) was discovered on September 11 2010 at optical wavelengths [98,99]. No γ-rays were detected. The value used for the distance, 5.7 ± 0.4 kpc was obtained using resolved radio images [48].

The radio light curve is double peaked, with the second peak adhering to our fit of the "Hubble Flow Model" (panel a) of Figure 3.8).

The first peak has, for the lower frequencies, brightness temperatures too high to be explained by thermal emission alone (see panel b)). During the rise to the first peak, the density rose as $t^{3.3}$ [80] which is not consistent with optically thick thermal ejecta. The residuals represented on panel d) clearly show an excess of flux compared to the thermal model during this peak.

During both peaks, the flux densities at the high frequencies were higher than those at lower frequencies. The higher frequencies reached it's higher flux value first, around day 198, while the higher flux densities for lower frequencies only happened around day 426 or 490.

Early resolved radio images reveal expanding bipolar flows, similar to what was seen in V959 Mon. These fade after sixteen months and reveal an inner structure more confined to the orbital plane. It is possible that the optically thick equatorial torus concealed some of the non-thermal radiation [48].

Internal shocks between multiple emission regions have already been proposed on the literature as the explanation [100]. The X-ray observations are also consistent with these shocks [100]. A time coincidence between the dust dip and the signs of shocks was also seen in this nova [48].

Previous fittings of the late time (t>141 days) radio data with the Hubble flow, derive an an ejecta mass of $M_{ej} = 1.7 \times 10^{-4} M_{\odot}$ and a electron temperature of $T_e = 1.1 \times 10^4$ K, keeping fixed the distance at $d = 6$ kpc and the maximum expansion velocity at $v_{exp} = 1500$km s^{-1} [48].

On our fit we fix the distance at $d = 5.7$ kpc and the electron temperature at $T_e = 10^4$ K. Our derived ejecta mass, $M_{ej} = \left(2.28^{+0.09}_{-0.20}\right) \times 10^{-4} M_{\odot}$ and the maximum expansion velocity, $v_{exp} = 2259^{+87}_{-221}$ kms^{-1} are higher than the previous fit.

In [48], a fitting of the early time (t<141 days) light curve is also provided, using a thermal model from [55] that models the shock as a fast wind of 12 days with velocity $v = 2100$km s^{-1} and mass $M = 0.8 \times 10^{-4} M_{\odot}$ with a shell with velocity $v = 1300$km s^{-1} with mass $M_{ej} = 1 \times 10^{-4} M_{\odot}$. Post-shock this results in an expansion velocity of $v_{exp} = 1500$km s^{-1} and a total ejecta mass of $M_{ej} \sim 1.8 \times 10^{-4} M_{\odot}$ [48]. These values are consistent with the values obtained for the late-time data but does not provide a good fit for the early time light curve when the distance is 6 kpc. This is a further sign that synchrotron emission, at least in part, generated the early time flare.

3.2 Discussion

Our models replicated well the observations at later times when the thermal component is clearly the dominant component. At early times, it was striking to see relative contribution of non-thermal component to the observed radio light curves. This is expected, as the "Hubble Flow Model" does not account for complex morphologies previously seen on some of these novae [8,89,90], as well as the possibility of clumping of the expelled material, presuming an

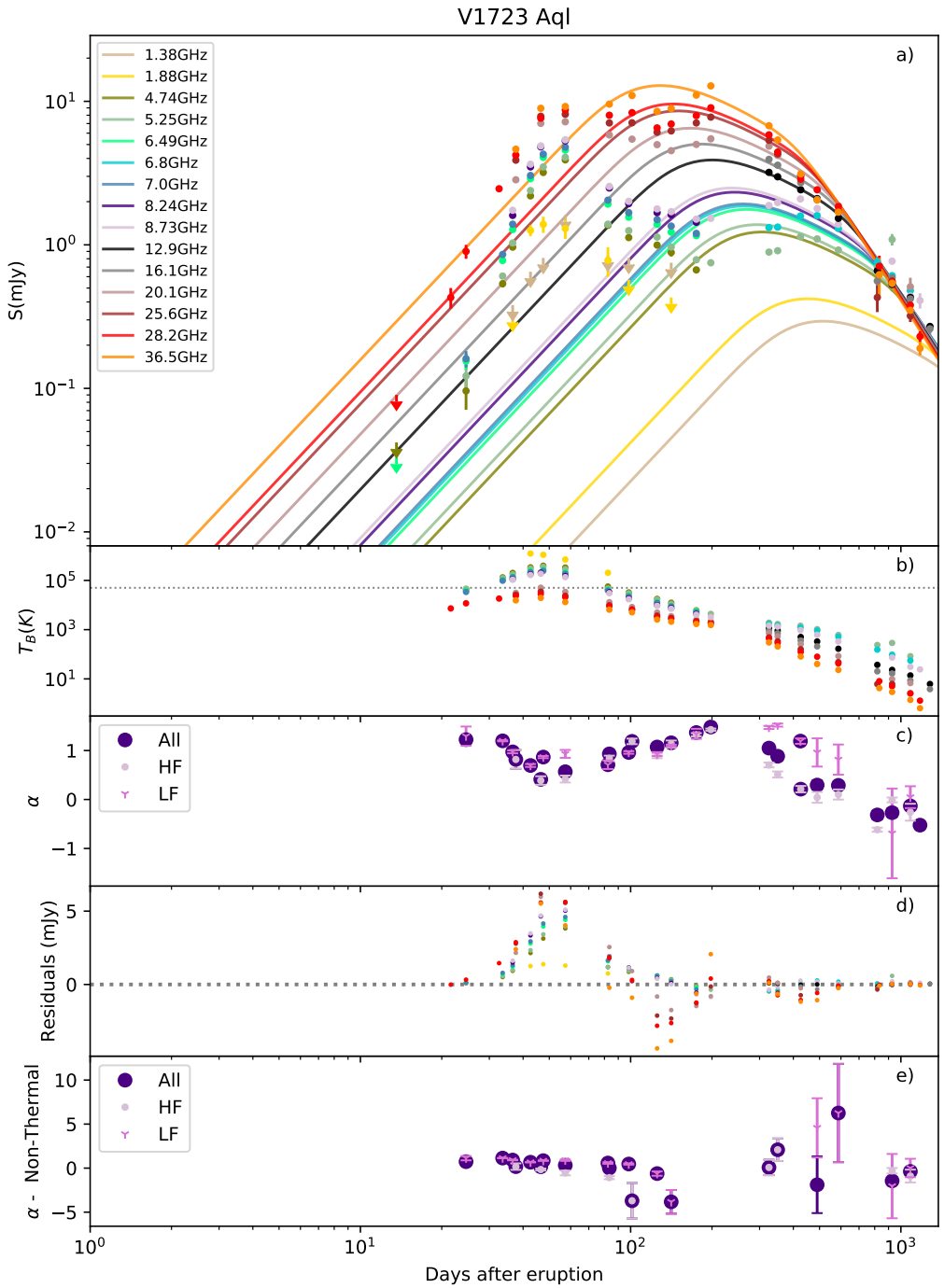

Figure 3.8: As Figure 3.1 but for V1723 Aql

instantaneous and homogeneous mass ejection that we know is not true based on our findings and other research.

Of the 7 novae in this study, 3 show clear double peaked radio curves (V1324 Sco, V357 Mus and V1723 Aql) with a first peak within 100 days. We attribute the first peak to non-thermal emission whose emission starts decreasing while the thermal emission has not yet reached its peak, producing a dip in the radio curve. In these curves, the model underestimates the emission during the first peak, as predicted if the non-thermal component is dominant during this stage. In the remaining 4 novae the thermal and synchrotron contributions appear to blur together into a single radio maximum. However,the fitting was able to decouple the two components in 3 of these novae (V959 Mon, V5589 Sgr and V5668 Sgr), as can be seen by the residuals plot (Figures 3.1, 3.7 and 3.3).

Brightness temperatures higher than 5×10^4 in at least some of the frequencies were seen in 5 of the studied novae, with the remaining 2 (V5668 Sgr and V906 Car) nevertheless showing values higher than the predicted for thermal emission only ($T_B > 10^4$).

We can safely establish that the non-thermal component is more dominant on the lower frequencies and in most of the novae studied is the primary emission mechanism in radio wavelengths for the first 100 days.

It was challenging to extract information from the spectral index evolution due to a lack of experimental points for the same day on multiple frequencies and the blending between thermal and non-thermal emission. In addiction, not all frequencies become optically thin at the same time, and therefore do not present the same spectral index behavior. In this work we tried to correct that by calculating the index considering the high and low frequencies independently. However, the use of a spectral break and doing the fit using broken power law models may be more adequate. This later method has been used in the study of V1723 Aql [48].

Dust dips or correlations between the dust formation and the γ-ray detection are seen on 5 of the 7 novae (V1324 Sco, V5668 Sgr, V357 Mus, V906 Car and V1723 Aql), which strengths the correlation between non-thermal emission, shocks and dust formation.

To study potential correlations between the γ-ray luminosity (Table 3.2) and the parameters of our model (distance, filling factor, maximum expansion velocity and ejecta mass) we did a plot of its values in function of the luminosity (Figure 3.9).

The correlation between γ-ray luminosity and distance has been extensively studied with no correlation found [12]. Our results (Figure 3.9) confirm that conclusion. The plot of our derived filling factor in function of the γ-ray luminosity does not show signs of any trend either.

The internal shock model predicts an increase in γ-ray luminosity with ejecta mass and velocity [12] but we observe the opposite behavior which indicates that the model needs further studies.

The correlation between γ-ray luminosity and v_{exp} seems to show a promising trend with lower velocities novae having higher γ-ray luminosity. However, the proposal of an explanation is beyond the scope of this work.

Finally, the correlation between γ-ray luminosity and ejecta mass is very promising. Ejecta masses seem to be inversely correlated with γ-ray luminosities. The outlier is V906 Car, whose mass is higher than the other novae with a considerable error bar. If however, the mass is an order of magnitude lower as derived by the previous fit on the literature ($M_{ej} \gtrsim 2 \times 10^{-4} M_\odot$ or $M_{ej} \gtrsim 9 \times 10^{-5} M_\odot$ depending on the ejection date) [58], this point would align with the overall trend. A deeper study of this nova with the inclusion of the date of the delayed ejection as a free parameter may allow a better estimation of its ejecta mass.

We may explain the decrease in γ-ray luminosity with more ejecta mass as due to the

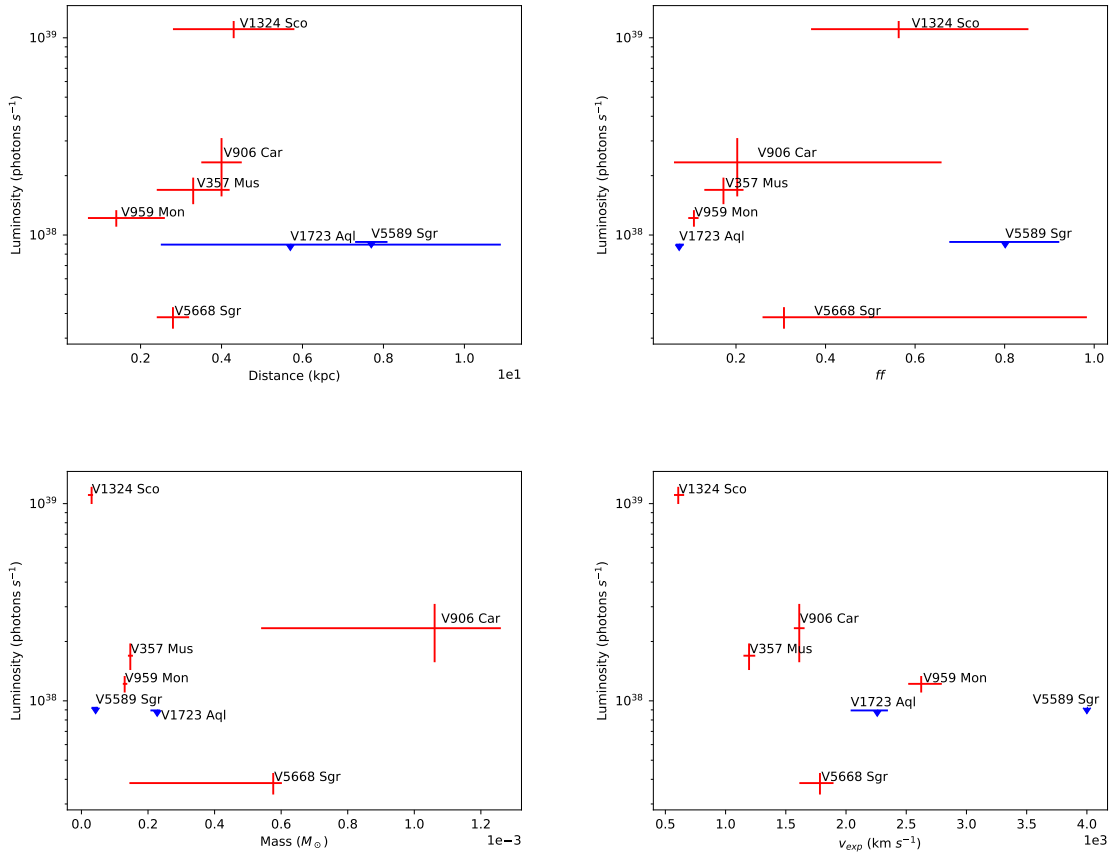

Figure 3.9: Relationships between γ-ray luminosity and the parameters of the thermal model fit. Relationship between γ-ray luminosity and the distance on the literature (top left). Relationship between γ-ray luminosity and the filling factor derived (top right). Relationship between γ-ray luminosity and the mass of the ejecta M derived (bottom left). Relationship between γ-ray luminosity and the maximum expansion velocity v_{exp} derived (bottom right).

---

attenuation by a dense column of dust or gas. This implies that the the location of the origin of the γ-rays needs to be rethought. The origin of this emission can not be on the outward of the ejecta where no dense material is present.

The sites of dust formation in novae remains poorly understood. Further observations on the IR and millimeter wavelengths may help to clarify it [12]. The increase in sensitivity on the detection of radio wavelengths brought by the planned SKA (Square Kilometer Array) telescope will also increase the resolution allowing us to pin point where γ–ray emission arises [101, 102].

The absence of γ-ray energies above 100-MeV in non-detected γ-ray novae has already been postulated to be due to photon-atom interactions absorption [54]. In addition, the absorption of electromagnetic emission by the dust has already been proposed for X-ray emission and it is used to explain the lack of detection of hard X-rays that should have been produced in the shocks in some of the novae [103, 104].

We predict that the intensity I of γ-ray emission detected has a decaying exponential relationship of the form

$$I = I_0 \exp(bM_{ej}) \tag{3.2}$$

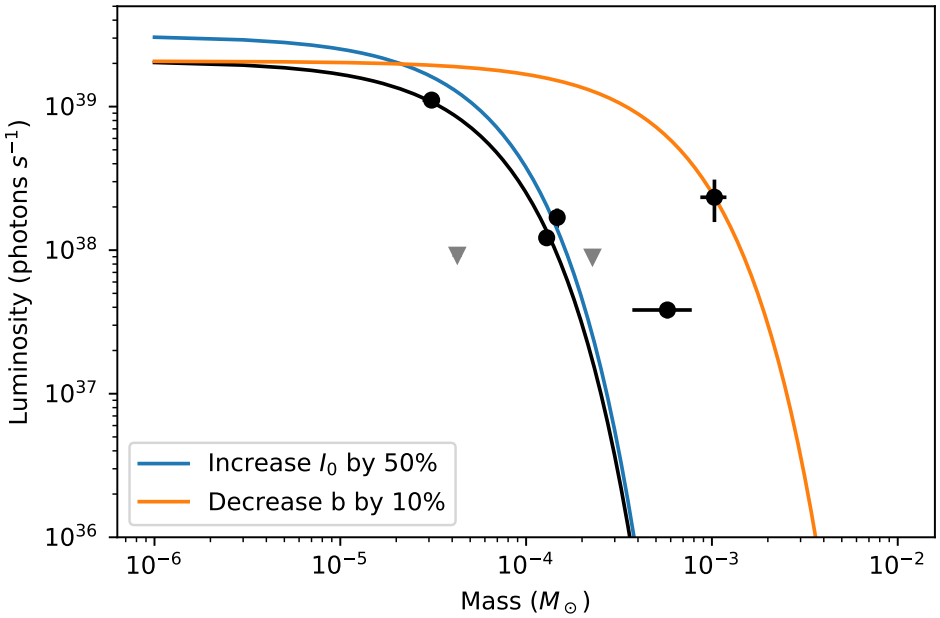

Figure 3.10: Plot of the mass as a function of the γ-ray luminosity (in black circles) or the upper limits of detection (in grey arrows) in a log scale superimposed with the best fit curve (black line) and the curve if we increase I_0 by 50 % or decrease b by 10% (blue and orange line respectively).

---

where I_0 represents the intensity before the interaction with the material, M_{ej} the ejecta mass and b a parameter that relates to the density and size of the material and its attenuation and scattering power.

We preformed a fit using the 4 novae with the best results by visual inspection (V959 Mon, V1324 Sco, V5668 Sgr and V357 Mus) to get preliminary values on these parameters. The resulting plot can be seen on Figure 3.10. The best fit parameters are:

$$I_0 = 2.072 \times 10^{39} \text{ photons } s^{-1} \qquad b = -2.111 \times 10^4 \ M_\odot^{-1} \tag{3.3}$$

Using a monoatomic energy approximation, we consider that all photons are emitted with an energy of 10^3 MeV, so this I_0 corresponds to a intensity of 3.21×10^{36} erg/s. The current expectation is that the energies emitted at γ-ray wavelengths are much smaller than the bolometric output of novae [12], which is consistent with the result above.

Chapter 4

Conclusions and Future Work

The novae analyzed in this dissertation display evidence of non-thermal emission, such as an excess of emission relative to the thermal model prediction, high brightness temperatures, and multiple-peaked radio light curves.

It was clearly evident that a one model fit to the data was not adequate. Notwithstanding, we found good fits to the data at later times, when the contribution from the non-thermal is reduced and the ejecta become optically thin thermal emission. At earlier times, the thermal emission model fails to predict the first peak, lending further support to non-thermal emission origin, on the double peaked radio curves.

The non-thermal component is found to be more dominant at lower frequencies, and the predominant emission mechanism in radio wavelengths over the first 100 days in most of the novae studied.

The best fit parameters from the thermal models were then compared with the gamma-ray luminosity to identify any correlations. A highly promising inverse correlation was identified between γ-ray luminosity and ejecta mass. This result may challenge the prediction of the internal shock model [12]: the more massive the ejecta the more gamma-ray luminosity we should expect. This preliminary results warrants further investigation.

The inverse correlation phenomena appears to be due to a thick column of dust or gas attenuating the γ-ray photons, such that the measured γ-ray intensity I will decline exponentially with the mass of ejecta such that $I = I_0 \exp(bM_{ej})$, where M_{ej} is the ejected mass and I_0 is the gamma-ray intensity before attenuation. The presence of such attenuation suggests that the origin of γ-rays must be reconsidered since the source of this emission cannot be on the ejecta's outer side, where there is no dense material to create an attenuation screen. Preliminary analysis of this exponential relationship, based on a fit using 4 novae with the best results by visual inspection (V959 Mon, V1324 Sco, V5668 Sgr, and V357 Mus), found that the intensity before interaction with the material was $I_0 = 2.072 \times 10^{39}$ photons s^{-1}. The derived value of I_0 is consistent with the expectation that the energies emitted at γ-ray wavelengths are much smaller than the bolometric output of novae [12].

Further analysis with more novae, improved modeling procedures with parameters such as clumping, and delayed ejections, as well as different ejected mass density profiles will contribute towards more established values for the mass. Another important factor is the better determination of the distance that will solidify the calculation of the γ-ray luminosities, this should be achieved with upcoming GAIA data releases as their parallax determination improve [105, 106].

Multiwavelength observations are crucial to a complete understanding of the nova eruption. The All-Sky Automated Survey for Supernovae (ASAS-SN) already underway will increase the number of novae detected in the next years [4]. The predicted discovery of

a larger sample of novae by SKA will also allow a more statistically significant study. In addition, the predicted increase in sensitivity and resolution on the detection of radio wavelengths by this telescope will help disentangle the location of shocks, γ-ray emission and dust formation [101, 102] with help from high-resolution IR and millimeter observations [12, 49]. If shocks largely occur in the orbital plane, we anticipate that the shocked gas' optical and X-ray signatures vary with orbital inclination [12]. The explanation behind the observed suppression of hard X-rays in comparison to what we anticipated to measure based on the strength of shocks would also aid our understanding of shocks.

As future work, the implementation of the clumping factor described on section 1.4 is of paramount importance, since multiple observational studies detect small clumps on the nova shell [49]. Furthermore, the introduction of the date of ejection, to mimic a delayed ejection scenario, as a free parameter in the `emcee` code could also allow a better fit, as multiple novae show signs of a delayed ejection. We also propose the inclusion of a weight factor between different frequencies, given that lower frequencies have a higher contribution from non-thermal emission and therefore should have a lower weight in a thermal model. Finally, the addition of a non-thermal component model to our thermal model would allow a much better fit.

Bibliography

[1] M. Bode and A. Evans. *Classical Novae*. Cambridge University Press, 2008.

[2] R. M. Hjellming, C. M. Wade, N. R. Vandenberg, and R. T. Newell. Radio emission from nova shells. *The Astronomical Journal*, 84:1619, oct 1979.

[3] Cecilia Helena Payne-Gaposchkin. *The Galactic Novae*. Amsterdam, North-Holland Pub. Co.; New York, Interscience Publishers, 1957.

[4] E. Aydi et.al. Early Spectral Evolution of Classical Novae: Consistent Evidence for Multiple Distinct Outflows. *The Astrophysical Journal*, 905(1):62, dec 2020.

[5] A R Taylor, R J Davis, R W Porcas, and M F Bode. VLBI observations of RS Oph - a recurrent nova with non-spherical ejection. *Monthly Notices of the Royal Astronomical Society*, 237(1):81–91, mar 1989.

[6] B D Metzger, T Finzell, I Vurm, R Hascoët, A M Beloborodov, and L Chomiuk. Gamma-ray novae as probes of relativistic particle acceleration at non-relativistic shocks. *Monthly Notices of the Royal Astronomical Society*, 450(3):2739–2748, may 2015.

[7] Andrey Vlasov, Indrek Vurm, and Brian D. Metzger. Shocks in nova outflows - II. Synchrotron radio emission. *Monthly Notices of the Royal Astronomical Society*, 463(1):394–412, 2016.

[8] Laura Chomiuk et. al. Binary orbits as the driver of γ-ray emission and mass ejection in classical novae. *Nature*, 514(7522):339–342, 2014.

[9] Timothy Cunningham, William M. Wolf, and Lars Bildsten. Photoionization heating of nova ejecta by the post-outburst supersoft source. *The Astrophysical Journal*, 803(2):1–7, apr 2015.

[10] Andrea M. Derdzinski, Brian D. Metzger, and Davide Lazzati. Radiative shocks create environments for dust formation in classical novae. *Monthly Notices of the Royal Astronomical Society*, 469(2):1314–1329, aug 2017.

[11] A. Franckowiak, P. Jean, M. Wood, C. C. Cheung, and S. Buson. Search for gamma-ray emission from Galactic novae with the Fermi -LAT. *Astronomy and Astrophysics*, 609:120, jan 2018.

[12] Laura Chomiuk, Brian D. Metzger, and Ken J. Shen. New Insights into Classical Novae. *Annual Review of Astronomy and Astrophysics*, 59:391–444, 2021.

[13] Daniel Foreman-Mackey, David W. Hogg, Dustin Lang, and Jonathan Goodman. emcee: The MCMC Hammer. *Publications of the Astronomical Society of the Pacific*, 125(925):306–312, feb 2012.

[14] Jonathan Goodman and Jonathan Weare. Ensemble samplers with affine invariance. *Communications in Applied Mathematics and Computational Science*, 5(1):65–80, 2010.

[15] J José. Classical nova explosions-hydrodynamics and nucleosynthesis. Technical report, 2012.

[16] S. Starrfield, C. Iliadis, and W. R. Hix. The Thermonuclear Runaway and the Classical Nova Outburst. *Publications of the Astronomical Society of the Pacific*, 128(963):051001, apr 2016.

[17] Robert D. Gehrz, James W. Truran, Robert E. Williams, and Sumner Starrfield. Nucleosynthesis in Classical Novae and Its Contribution to the Interstellar Medium. *Publications of the Astronomical Society of the Pacific*, 110(743):3–26, jan 1998.

[18] O. Yaron, D. Prialnik, M. M. Shara, and A. Kovetz. An Extended Grid of Nova Models. II. The Parameter Space of Nova Outbursts. *The Astrophysical Journal*, 623(1):398–410, apr 2005.

[19] Attay Kovetz and Dina Prialnik. CNO abundances resulting from diffusion in accreting nova progenitors. *The Astrophysical Journal*, 291:812, 1985.

[20] Nikolaus Vogt, Susanne M. Hoffmann, and Claus Tappert. On the possibilities of classical nova identifications among historical Far Eastern guest star observations. *Astronomische Nachrichten*, 340(8):752–759, oct 2019.

[21] Mansi M. Kasliwal. Systematically bridging the gap between novae and supernovae. *Proceedings of the International Astronomical Union*, 7(S281):9–16, jan 2013.

[22] Massimo Della Valle and Luca Izzo. Observations of galactic and extragalactic novae. *Astronomy and Astrophysics Review*, 28(1), 2020.

[23] A W Shafter. The Galactic Nova Rate Revised. *The Astrophysical Journal*, 834(2):196, 2017.

[24] Koji Mukai and Jennifer L. Sokoloski. The new science of novae. *Physics Today*, 72(11):38–44, 2019.

[25] M. Della Valle, A. Bianchini, M. Livio, and M. Orio. On the possible existence of two classes of progenitors for classical novae. *Astronomy and astrophysics (Berlin. Print)*, 266(1):232–236, 1992.

[26] M. F. Bode. The outbursts of classical and recurrent novae. *Astronomische Nachrichten*, 331(2):160–168, feb 2010.

[27] M. J. Darnley, V. A. R. M. Ribeiro, M. F. Bode, R. A. Hounsell, and R. P. Williams. On The Progenitors Of Galactic Novae. *The Astrophysical Journal*, 746(1):61, jan 2012.

[28] GC Anupama. The Recurrent Nova Class of Objects. *RS Ophiuchi (2006) and the Recurrent Nova*, 401(2006):31–41, 2008.

[29] Bradley E. Schaefer. Comprehensive photometric histories of all known galactic recurrent novae. *Astrophysical Journal, Supplement Series*, 187(2):275–373, 2010.

[30] Ashley Pagnotta and Bradley E. Schaefer. Identifying and quantifying recurrent novae masquerading as classical novae. *Astrophysical Journal*, 788(2), 2014.

[31] M Hernanz and J José. The recurrent nova RS Oph: A possible scenario for type Ia supernovae, 2008.

[32] M. Zorotovic, M. R. Schreiber, B. T. Gänsicke, M. Zorotovic, M. R. Schreiber, and B. T. Gänsicke. Post common envelope binaries from SDSS. XI. The white dwarf mass distributions of CVs and pre-CVs. *A&A*, 536:A42, 2011.

[33] T. P. G. Wijnen, M. Zorotovic, and M. R. Schreiber. White dwarf masses in cataclysmic variables. *A&A*, 577:A143, may 2015.

[34] Rodrigo C V Coelho, Maurício O Calvão, Ribamar R R Reis, and Beatriz B Siffert. Standardization of type Ia supernovae. *European Journal of Physics*, 36(1):015007, nov 2014.

[35] Dan Maoz, Filippo Mannucci, and Gijs Nelemans. Observational Clues to the Progenitors of Type Ia Supernovae. *ARA&A*, 52:107–170, August 2014.

[36] J Washington, L Chomiuk, and S Sarbadhicary. Constraining Type Ia Supernova Progenitor Environments with Late-Time Radio Observations. In *American Astronomical Society Meeting Abstracts #235*, volume 235 of *American Astronomical Society Meeting Abstracts*, page 307.11, jan 2020.

[37] Peter Lundqvist, Esha Kundu, Miguel A. Pérez-Torres, Stuart D. Ryder, Claes Ingvar Björnsson, Javier Moldon, Megan K. Argo, Robert J. Beswick, Antxon Alberdi, and Erik C. Kool. The deepest radio observations of nearby type IA supernovae: Constraining progenitor types and optimizing future surveys, jan 2020.

[38] R. Hounsell et. al. Exquisite Nova Light Curves from the Solar Mass Ejection Imager (SMEI). *The Astrophysical Journal*, 724(1):480–486, nov 2010.

[39] E R Seaquist and John Palimaka. Thick inhomogeneous shell models for the radio emission from Nova Serpentis 1970. *The Astrophysical Journal*, 7813:781–787, 1977.

[40] J. S. Gallagher and S. Starrfield. Theory and Observations of Classical Novae. *Annual Review of Astronomy and Astrophysics*, 16(1):171–214, sep 1978.

[41] R. A Hjellming. Radio Emission from the Stars and the Sun. In A. R. Taylor and J. M. Paredes., editors, *Radio Emission from the Stars and the Sun*, page 174, Barcelona, Spain, 1996. Astronomical Society of the Pacific (January 1, 1996).

[42] Joachim Krautter, Charles E. Woodward, Michael T. Schuster, Robert D. Gehrz, Terry J. Jones, Kunegunda Belle, A. Evans, S. P. S. Leyers, Sumner Starrfield, James Truran, and Matthew A. Greenhouse. Hubble Space Telescope NICMOS Observations of Classical Nova Shells. *The Astronomical Journal*, 124(5):2888–2898, nov 2002.

[43] Brian Warner. *Cataclysmic Variable Stars*. Cambridge University Press, dec 1995.

[44] E. Mason, M. Della Valle, R. Gilmozzi, G. Lo Curto, and R. E. Williams. Early decline spectra of nova SMC 2001 and nova LMC 2002. *Astronomy & Astrophysics*, 435(3):1031–1042, jun 2005.

[45] B. D. Metzger, D. Caprioli, I. Vurm, A. M. Beloborodov, I. Bartos, and A. Vlasov. Novae as Tevatrons: Prospects for CTA and IceCube. *Monthly Notices of the Royal Astronomical Society*, 457(2):1786–1795, 2016.

[46] Ian Heywood. *Radio Emission From Classical Novae*. PhD thesis, 2004.

[47] David C Abbott and John H Bieging. Mass Loss From Very Luminous Ob Stars And The Cygnus Superbubble. *The Astrophysical Journal*, 250:645–659, 1981.

[48] Jennifer H.S. Weston, J. L. Sokoloski, Brian D. Metzger, Yong Zheng, Laura Chomiuk, Miriam I. Krauss, Justin D. Linford, Thomas Nelson, Amy J. Mioduszewski, Michael P. Rupen, Tom Finzell, and Koji Mukai. Non-thermal radio emission from colliding flows in classical nova V1723 Aql. *Monthly Notices of the Royal Astronomical Society*, 457(1):887–901, 2016.

[49] Marcos P Diaz, Zulema Abraham, Valério A R M Ribeiro, Pedro P B Beaklini, and Larissa Takeda. The structure of a recent nova shell as observed by ALMA. *Monthly Notices of the Royal Astronomical Society: Letters*, 480(1):L54–L57, oct 2018.

[50] A. R. Taylor, E. R. Seaquist, J. M. Hollis, and S. R. Pottasch. The unusual radio outburst of Nova Vulpeculae 1984 No 2. *A&A*, 183:38–46, 1987.

[51] M. A. J. Snijders, T. J. Batt, P. F. Roche, M. J. Seaton, D. C. Morton, T. A. T. Spoelstra, and J. C. Blades. Nova Aquilae 1982. *Monthly Notices of the Royal Astronomical Society*, 228(2):329–376, sep 1987.

[52] Malcolm S. Longair. *High Energy Astrophysics*. Cambridge University Press, Cambridge, 2010.

[53] Richard J. Strope, Bradley E. Schaefer, and Arne A. Henden. Catalog Of 93 Nova Light Curves: Classification And Properties. *The Astronomical Journal*, 140(1):34, may 2010.

[54] M. Ermann et. al. Fermi establishes classical novae as a distinct class of gamma-ray sources: The Fermi-LAT collaboration. *Science*, 345(6196):554–558, aug 2014.

[55] Brian D. Metzger, Romain Hascoët, Indrek Vurm, Andrei M. Beloborodov, Laura Chomiuk, J. L. Sokoloski, and Thomas Nelson. Shocks in nova outflows - I. Thermal emission. *Monthly Notices of the Royal Astronomical Society*, 442(1):713–731, 2014.

[56] Jennifer H.S. Weston, J. L. Sokoloski, Laura Chomiuk, Justin D. Linford, Thomas Nelson, Koji Mukai, Tom Finzell, Amy Mioduszewski, Michael P. Rupen, and Frederick M. Walter. Shock-powered radio emission from V5589 Sagittarii (Nova Sgr 2012 #1). *Monthly Notices of the Royal Astronomical Society*, 460(3):2687–2697, 2016.

[57] Thomas Finzell et. al. A Detailed Observational Analysis of V1324 Sco, the Most Gamma-Ray-luminous Classical Nova to Date. *The Astrophysical Journal*, 852(2):108, 2018.

[58] Elias Aydi et. al. Direct evidence for shock-powered optical emission in a nova. *Nature Astronomy*, 4(8):776–780, 2020.

[59] F. Healy, T. J. O'Brien, R. Beswick, A. Avison, and M. K. Argo. Multi-epoch radio imaging of γ-ray Nova V959 Mon. *Monthly Notices of the Royal Astronomical Society*, 469(4):3976–3983, 2017.

[60] A. A. Abdo et. al. Gamma-ray emission concurrent with the nova in the symbiotic binary V407 cygni. *Science*, 329(5993):817–821, aug 2010.

[61] Paul J. Morris, Garret Cotter, Anthony M. Brown, and Paula M. Chadwick. Gamma-ray novae: Rare or nearby? *Monthly Notices of the Royal Astronomical Society*, 465(1):1218–1226, 2017.

[62] J. D. Linford, L. Chomiuk, T. Nelson, T. Finzell, F. M. Walter, J. L. Sokoloski, K. Mukai, A. J. Mioduszewski, A. J. van der Horst, J. H. S. Weston, and M. P. Rupen. The Peculiar Multiwavelength Evolution Of V1535 Sco. *The Astrophysical Journal*, 842(2):73, 2017.

[63] Thomas Nelson, Koji Mukai, Kwan-Lok Li, Indrek Vurm, Brian D. Metzger, Laura Chomiuk, J. L. Sokoloski, Justin D. Linford, Terry Bohlsen, and Paul Luckas. NuSTAR Detection of X-Rays Concurrent with Gamma-Rays in the Nova V5855 Sgr. *The Astrophysical Journal*, 872(1):86, 2019.

[64] Kwan Lok Li, Brian D. Metzger, Laura Chomiuk, Indrek Vurm, Jay Strader, Thomas Finzell, Andrei M. Beloborodov, Thomas Nelson, Benjamin J. Shappee, Christopher S. Kochanek, José L. Prieto, Stella Kafka, Thomas W.S. Holoien, Todd A. Thompson, Paul J. Luckas, and Hiroshi Itoh. A nova outburst powered by shocks. *Nature Astronomy*, 1(10):697–702, 2017.

[65] C. C. Cheung, P. Jean, S. N. Shore, L. Stawarz, R. H. D. Corbet, J. Knodlseder, S. Starrfield, D. L. Wood, R. Desiante, F. Longo, G. Pivato, and K. S. Wood. Fermi LAT Gamma-ray Detections of Classical Novae V1369 Centauri 2013 and V5668 Sagittarii 2015. (2), 2016.

[66] Elad Steinberg and Brian D Metzger. Internal shocks from variable outflows in classical novae. *Monthly Notices of the Royal Astronomical Society*, 491(3):4232–4246, 2020.

[67] C. D. Gill and T. J. O'Brien. Deep optical imaging of nova remnants: a southern sky sample. *Monthly Notices of the Royal Astronomical Society*, 300(1):221–232, oct 1998.

[68] A. J. Slavin, T. J. O'Brien, and J. S. Dunlop. A deep optical imaging study of the nebular remnants of classical novae. *Monthly Notices of the Royal Astronomical Society*, 276(2):353–371, sep 1995.

[69] V. A. R. M. Ribeiro, L. Chomiuk, U. Munari, W. Steffen, N. Koning, T. J. O'Brien, T. Simon, P. A. Woudt, and M. F. Bode. Radio Frequency Models Of Novae In Eruption. I. The Free–free Process In Bipolar Morphologies. *The Astrophysical Journal*, 792(1):57, aug 2014.

[70] C. W. Allen. *Astrophysical quantities*. 1963.

[71] L H Aller and W Liller. In Stars and stellar systems, eds Middlehurst. *BM & Aller, LH, volume*, 1968.

[72] T. Birmingham, J. Dawson, C. Oberman, and George Befki. *Radiation processes in plasmas*, volume 8. 1966.

[73] National Radio Astronomy Observatory. The karl g. jansky very large array. `https://science.nrao.edu/facilities/vla/`, 10 2021.

[74] CSIRO. Australia telescope national facility. `https://www.atnf.csiro.au/f`, 10 2021.

[75] W. B. Atwood, A. A. Abdo, M. Ackermann, W. Althouse, B. Anderson, M. Axelsson, L. Baldini, J. Ballet, D. L. Band, G. Barbiellini, J. Bartelt, D. Bastieri, B. M. Baughman, K. Bechtol, D. Bédérède, F. Bellardi, R. Bellazzini, B. Berenji, G. F. Bignami, D. Bisello, E. Bissaldi, R. D. Blandford, E. D. Bloom, J. R. Bogart, E. Bonamente, J. Bonnell, A. W. Borgland, A. Bouvier, J. Bregeon, A. Brez, M. Brigida, P. Bruel, T. H. Burnett, G. Busetto, G. A. Caliandro,

R. A. Cameron, P. A. Caraveo, S. Carius, P. Carlson, J. M. Casandjian, E. Cavazzuti, M. Ceccanti, C. Cecchi, E. Charles, A. Chekhtman, C. C. Cheung, J. Chiang, R. Chipaux, A. N. Cillis, S. Ciprini, R. Claus, J. Cohen-Tanugi, S. Condamoor, J. Conrad, R. Corbet, L. Corucci, L. Costamante, S. Cutini, D. S. Davis, D. Decotigny, M. DeKlotz, C. D. Dermer, A. de Angelis, S. W. Digel, E. do Couto e Silva, P. S. Drell, R. Dubois, D. Dumora, Y. Edmonds, D. Fabiani, C. Farnier, C. Favuzzi, D. L. Flath, P. Fleury, W. B. Focke, S. Funk, P. Fusco, F. Gargano, D. Gasparrini, N. Gehrels, F. X. Gentit, S. Germani, B. Giebels, N. Giglietto, P. Giommi, F. Giordano, T. Glanzman, G. Godfrey, I. A. Grenier, M. H. Grondin, J. E. Grove, L. Guillemot, S. Guiriec, G. Haller, A. K. Harding, P. A. Hart, E. Hays, S. E. Healey, M. Hirayama, L. Hjalmarsdotter, R. Horn, R. E. Hughes, G. Jóhannesson, G. Johansson, A. S. Johnson, R. P. Johnson, T. J. Johnson, W. N. Johnson, T. Kamae, H. Katagiri, J. Kataoka, A. Kavelaars, N. Kawai, H. Kelly, M. Kerr, W. Klamra, J. Knödlseder, M. L. Kocian, N. Komin, F. Kuehn, M. Kuss, D. Landriu, L. Latronico, B. Lee, S. H. Lee, M. Lemoine-Goumard, A. M. Lionetto, F. Longo, F. Loparco, B. Lott, M. N. Lovellette, P. Lubrano, G. M. Madejski, A. Makeev, B. Marangelli, M. M. Massai, M. N. Mazziotta, J. E. McEnery, N. Menon, C. Meurer, P. F. Michelson, M. Minuti, N. Mirizzi, W. Mitthumsiri, T. Mizuno, A. A. Moiseev, C. Monte, M. E. Monzani, E. Moretti, A. Morselli, I. V. Moskalenko, S. Murgia, T. Nakamori, S. Nishino, P. L. Nolan, J. P. Norris, E. Nuss, M. Ohno, T. Ohsugi, N. Omodei, E. Orlando, J. F. Ormes, A. Paccagnella, D. Paneque, J. H. Panetta, D. Parent, M. Pearce, M. Pepe, A. Perazzo, M. Pesce-Rollins, P. Picozza, L. Pieri, M. Pinchera, F. Piron, T. A. Porter, L. Poupard, S. Rainò, R. Rando, E. Rapposelli, M. Razzano, A. Reimer, O. Reimer, T. Reposeur, L. C. Reyes, S. Ritz, L. S. Rochester, A. Y. Rodriguez, R. W. Romani, M. Roth, J. J. Russell, F. Ryde, S. Sabatini, H. F. W. Sadrozinski, D. Sanchez, A. Sander, L. Sapozhnikov, P. M. Saz Parkinson, J. D. Scargle, T. L. Schalk, G. Scolieri, C. Sgrò, G. H. Share, M. Shaw, T. Shimokawabe, C. Shrader, A. Sierpowska-Bartosik, E. J. Siskind, D. A. Smith, P. D. Smith, G. Spandre, P. Spinelli, J. L. Starck, T. E. Stephens, M. S. Strickman, A. W. Strong, D. J. Suson, H. Tajima, H. Takahashi, T. Takahashi, T. Tanaka, A. Tenze, S. Tether, J. B. Thayer, J. G. Thayer, D. J. Thompson, L. Tibaldo, O. Tibolla, D. F. Torres, G. Tosti, A. Tramacere, M. Turri, T. L. Usher, N. Vilchez, V. Vitale, P. Wang, K. Watters, B. L. Winer, K. S. Wood, T. Ylinen, and M. Ziegler. The Large Area Telescope on the Fermi Gamma-Ray Space Telescope Mission. *The Astrophysical Journal*, 697(2):1071–1102, June 2009.

[76] J. D. Linford, V. A. R. M. Ribeiro, L. Chomiuk, T. Nelson, J. L. Sokoloski, M. P. Rupen, K. Mukai, T. J. O'Brien, A. J. Mioduszewski, and J. Weston. The Distance To Nova V959 Mon From VLA Imaging. *The Astrophysical Journal*, 805(2):136, may 2015.

[77] Aykut Özdönmez, Tolga Güver, Antonio Cabrera-Lavers, and Tansel Ak. The distances of the Galactic novae. *Monthly Notices of the Royal Astronomical Society*, 461(2):1177–1201, sep 2016.

[78] Laura Chomiuk, Justin D Linford, Elias Aydi, Keith W Bannister, Miriam I Krauss, Amy J Mioduszewski, Koji Mukai, Thomas J Nelson, Michael P Rupen, Stuart D Ryder, Jennifer L Sokoloski, Kirill V Sokolovsky, Jay Strader, Miroslav D Filipovic, Tom Finzell, Adam Kawash, Erik C Kool, Brian D Metzger, Miriam M Nyamai, Valerio A R M Ribeiro, Nirupam Roy, Ryan Urquhart, and Jennifer Weston. Classical Novae at Radio Wavelengths, 2021.

[79] A. C. Gordon, E. Aydi, K. L. Page, Kwan-Lok Li, L. Chomiuk, K. V. Sokolovsky, K. Mukai, and J. Seitz. Surveying the X-Ray Behavior of Novae as They Emit γ-Rays. *The Astrophysical Journal*, 910(2):134, apr 2021.

[80] Miriam I. Krauss, Laura Chomiuk, Michael Rupen, Nirupam Roy, Amy J. Mioduszewski, J. L. Sokoloski, Thomas Nelson, Koji Mukai, M. F. Bode, S. P.S. Eyres, and T. J. O'Brien. Expanded very large array nova project observations of the classical nova V1723 aquilae. *Astrophysical Journal Letters*, 739(1), 2011.

[81] C. C. Cheung, S. N. Shore, I. De Gennaro Aquino, S. Charbonnel, J. Edlin, E. Hays, R. H. D. Corbet, and D. L. Wood. Possible Association of the Gamma-ray Transient Fermi J0639+0548 with Nova Mon 2012. *The Astronomer's Telegram*, 4310:1, August 2012.

[82] U. Munari, S. Dallaporta, F. Castellani, P. Valisa, A. Frigo, L. Chomiuk, and V. A. R. M. Ribeiro. Photometric evolution, orbital modulation and progenitor of Nova Mon 2012. *Monthly Notices of the Royal Astronomical Society*, 435(1):771–781, oct 2013.

[83] R. M. Wagner, S. Dong, T. Bensby, J. Prieto, I. Bond, P. Tristram, D. Bennett, K. Wada, T. Sumi, A. Gould, and S. Starrfield. MOA 2012 BLG-320: Discovery and Observations of a Nova Candidate Towards the Galactic Bulge. *The Astronomer's Telegram*, 4157:1, June 2012.

[84] Thomas Finzell, Laura Chomiuk, Ulisse Munari, and Frederick M. Walter. Distance And Reddening Of The Enigmatic Gamma-ray-detected Nova V1324 Sco. *The Astrophysical Journal*, 809(2):160, 2015.

[85] J. Seach. Nova Sagittarii 2015 No. 2 = Pnv J18365700-2855420. *Central Bureau Electronic Telegrams*, 4080:1, March 2015.

[86] C C Cheung, P Jean, S N Shore, Ł Stawarz, R H D Corbet, J Knödlseder, S Starrfield, D L Wood, R Desiante, F Longo, G Pivato, and K S Wood. Fermi-LAT Gamma-ray Detections Of Classical Novae V1369 Centauri 2013 And V5668 Sagittarii 2015. *The Astrophysical Journal*, 826, 2016.

[87] Akito Tajitsu, Kozo Sadakane, Hiroyuki Naito, Akira Arai, Hideyo Kawakita, and Wako Aoki. The 7 Be ii Resonance Lines In Two Classical Novae V5668 Sgr And V2944 Oph. *The Astrophysical Journal*, 818(2):191, 2016.

[88] P. Molaro, L. Izzo, E. Mason, P. Bonifacio, and M. Della Valle. Highly enriched 7Be in the ejecta of Nova Sagittarii 2015 No. 2 (V5668 Sgr) and the Galactic 7Li origin. *Monthly Notices of the Royal Astronomical Society: Letters*, 463(1):L117–L121, nov 2016.

[89] D. P. K. Banerjee, Mudit K. Srivastava, N. M. Ashok, and V. Venkataraman. Near-infrared studies of the carbon monoxide and dust-forming Nova V5668 Sgr. *Monthly Notices of the Royal Astronomical Society: Letters*, 455(1):L109–L113, jan 2016.

[90] Justin Linford, Stephen Lawrence, Laura Chomiuk, Jennifer Sokoloski, Thomas Nelson, Koji Mukai, Michael Rupen, Amy Mioduszewski, Alexander van der Horst, and Adam Kawash. Intriguing Misalignment Between Radio and Optical Structures in Classical Nova V5668 Sgr. In *American Astronomical Society Meeting Abstracts #231*, volume 231 of *American Astronomical Society Meeting Abstracts*, page 414.02, jan 2018.

[91] Indrek Vurm and Brian D. Metzger. High-energy Emission from Nonrelativistic Radiative Shocks: Application to Gamma-Ray Novae. *The Astrophysical Journal*, 852(1):62, 2018.

[92] Thomas Siegert, Alain Coc, Laura Delgado, Roland Diehl, Jochen Greiner, Margarita Hernanz, Pierre Jean, Jordi José, Paolo Molaro, Moritz M.M. Pleintinger, Volodymyr Savchenko, Sumner Starrfield, Vincent Tatischeff, and Christoph Weinberger. Gamma-ray observations of Nova Sgr 2015 No. 2 with INTEGRAL. *Astronomy and Astrophysics*, 615:1–11, 2018.

[93] R. Kaufman, E. Guido, A. Noschese, P. Schmeer, A. Valvasor, A. Pearce, and E. O. Waagen. Nova Muscae 2018. *Central Bureau Electronic Telegrams*, 4473:1, January 2018.

[94] Kwan-Lok Li, Koji Mukai, Thomas Nelson, and Laura Chomiuk. The Fermi-LAT detection of PNV J11261220-6531086. *The Astronomer's Telegram*, 11201:1, January 2018.

[95] K. Z. Stanek, T. W. S. Holoien, C. S. Kochanek, J. V. Shields, T. A. Thompson, L. Chomiuk, J. Strader, B. J. Shappee, J. L. Prieto, Subo Dong, and M. Stritzinger. ASAS-SN Discovery of a Possible, Very Bright Galactic Nova ASASSN-18fv. *The Astronomer's Telegram*, 11454:1, March 2018.

[96] Thomas Nelson, Koji Mukai, J. L. Sokoloski, Brian Metzger, Laura Chomiuk, Justin Linford, and Indrek Vurm. NuSTAR detects X-rays from a deeply embedded shock in the Fermi-detected nova ASASSN-18fv. *The Astronomer's Telegram*, 11608:1, May 2018.

[97] S. Korotkiy, K. Sokolovsky, N. J. Brown, R. J. Gao, J. Seach, S. Kiytota, E. Guido, N. Howes, G. Sostero, L. Elenin, I. Molotov, R.A.A. Koff, M. Nissinen, K. Nishiyama, F. Kabashima, H. Koberger, W. Vollmann, and V. Gerke. Nova Sagittarii 2012 = PNV J17452791-2305213. *Central Bureau Electronic Telegrams*, 3089:1, April 2012.

[98] D. Balam, E. Y. Hsiao, and M. Graham. V1723 Aquilae = Nova Aquilae 2010. *IAU Circ.*, 9168:1, September 2010.

[99] M. Yamanaka, R. Itoh, and T. Komatsu. Nova Aquilae 2010. *IAU Circ.*, 9167:3, September 2010.

[100] Jennifer H S Weston, Jennifer L J.L. Sokoloski, Yong Zheng, Laura Chomiuk, Amy Mioduszewski, Koji Mukai, Michael P M.P. Rupen, Miriam I M.I. Krauss, Nirupam Roy, Thomas Nelson, J.H.S. Weston, Jennifer L J.L. Sokoloski, Yong Zheng, Laura Chomiuk, Amy Mioduszewski, Koji Mukai, Michael P M.P. Rupen, Miriam I M.I. Krauss, Nirupam Roy, and Thomas Nelson. Shocks and Ejecta Mass: Radio Observations of Nova V1723 Aql. In P. A. Woudt and V.A.R.M. Ribeiro, editors, *Stellar Novae: Past and Future Decades*, volume 490 of *Astronomical Society of the Pacific Conference Series*, page 339, dec 2014.

[101] Tim O'Brien, Michael Rupen, Laura Chomiuk, Valerio Ribeiro, Michael Bode, Jennifer Sokoloski, and Patrick Woudt. Thermal radio emission from novae & symbiotics with the Square Kilometre Array. 2015.

[102] Valério A R M Ribeiro, João G Rosa, and Sonia Antón. Astrophysical Transients. In *Portuguese SKA White Book*. UA Editora – Universidade de Aveiro, 2020.

[103] Indrek Vurm, Brian D. Metzger, Indrek Vurm, and Brian D. Metzger. High-energy Emission from Nonrelativistic Radiative Shocks: Application to Gamma-Ray Novae. *The Astrophysical Journal*, 852(1):62, jan 2018.

[104] Nasa Goddard. The Early X-ray Emission From V382 Velorum (nova Velorum 1999) : An Internal Shock Model. *The Astrophysical Journal*, 551:1024–1030, 2001.

[105] X. Luri, A. G. A. Brown, L. M. Sarro, F. Arenou, C. A. L. Bailer-Jones, A. Castro-Ginard, J. de Bruijne, T. Prusti, C. Babusiaux, and H. E. Delgado. Gaia Data Release 2. Using Gaia parallaxes. *Astronomy & Astrophysics*, 616:A9, aug 2018.

[106] Bradley E. Schaefer and Bradley E. The distances to Novae as seen by Gaia. *Monthly Notices of the Royal Astronomical Society*, 481(3):3033–3051, dec 2018.

Appendix A

Thermal Code and emcee Implementation (in Python)

```
def radii(t,vexp,ff):
    r2=vexp*t
    r1=ff*r2
    return r1,r2

def functiongff(Te,nu):
    gff=(3.**(1./2.)/cst.pi) * (17.7+np.log(Te**(3./2.)/nu))
    return gff

def functionB(nu,Te):
    B=((2.*h*nu**3)/(c**2))/(np.exp(h*nu/(kb*Te))-1.)
    return B

def functionG(r,a):
    G=(1/a**2)*((r**2-a**2)**(1/2)/r**2+(1/a)*np.arccos(a/r))
    return G

def functionF(nu,Te,M):
    gff=functiongff(Te,nu)
    F=(1/Cst)**2 * np.exp(-h*nu/(kb*Te)) * (M/(4.*cst.pi))**2
     *(5.4E-39*Te**(-0.5)*gff)
    return F

def integrand(a,d,vexp,ff,M,Te,t,nu):
    (r1,r2)=radii(t,vexp,ff)
    F=functionF(nu,Te,M)
    B=functionB(nu,Te)
    if a <= r1/100.:
        Tau3 = (F/B) * (2.0/3.0) * (1.0 / r1**3 - 1.0 / r2**3)  /
        ((r2 - r1)**2)
        if Tau3 > 50.:
            return a
        else: return a*(1-np.exp(-Tau3))
    elif a<=r1 :
        Gr1 = functionG(r1,a)
        Gr2 = functionG(r2,a)
        Tau1=(F/B)*(Gr2-Gr1)/((r2-r1)**2)
```

```
        if Tau1 > 50.:
            return a
        else: return a*(1-np.exp(-Tau1))
    else: #a>r1
        Gr2 = functionG(r2,a)
        Tau2=(F/B)*Gr2/((r2-r1)**2)
        if Tau2 > 50.:
            return a
        else: return a*(1-np.exp(-Tau2))

def functionS(d,vexp,ff,M,Te,t,nu):
    (r1,r2)=radii(t,vexp,ff)
    integr,err=integrate.quad(integrand,0,r2, epsabs=1.49e-02,
    epsrel=1.49e-02, limit=200,args=(d,vexp,ff,M,Te,t,nu))
    B=functionB(nu,Te)
    S=2*cst.pi*B/d**2*integr
    return S

def thermalmodel(d,vexp,ff,M,Te,tdata,nu):
    d = 10**d*3.086e21
    M = 10**M*1.99e33
    Te=10**Te
    vexp = 10**vexp*1.e5
    S=np.zeros(len(tdata))
    for n in range(len(tdata)):
        t=tdata[n]/1.157E-5
        S[n]=functionS(d,vexp,ff,M,Te,t,nu)
    S=S*1E26
    return S

#-----------------------------------------------------------------------

def whats_theta(theta):
    k=0
    var = []
    for i in range(len(prior)):
        if prior[i] != -99:
            var.append(theta[k])
            k += 1
        else: var.append(fixed[i])

    return var

#-----------------------------------------------------------------------

def log_likelihood(theta):

    d,vexp,ff,M,Te,log_f = whats_theta(theta)

    L=0
    for i in range(len(nuvalues)):
        model=thermalmodel(d,vexp,ff,M,Te,tdata,nuvalues[i])
        sigma2_LF = Serr_LF ** 2 + model ** 2 * np.exp(2 * log_f)
        L+=-np.sum(np.log(1+(Sdata_LF - model) ** 2 / (2*sigma2_LF))
        +np.log(sigma2_LF))
```

```
    return L

def log_prior(theta):
    params = whats_theta(theta)
    lp = 0.0
    for i in range(len(params)):
        if not (p_limits[i][0] < params[i] < p_limits[i][1]):
            return -np.inf
    mmu = 0.
    msigma = 10.
    for i in range(len(params)):
        lp -= 0.5 * ((params[i] - mmu) / msigma)**2
    return lp

def log_probability(theta):
    lp = log_prior(theta)
    if not np.isfinite(lp):
        return -np.inf
    return lp + log_likelihood(theta)

#-----------------------------------------------------------------------

filename = "samples"+run+".h5"
backend = emcee.backends.HDFBackend(filename)
backend.reset(nwalkers, ndim)

pos=guess+1e-4 * np.random.randn(nwalkers,ndim)

with Pool() as pool:
    sampler = emcee.EnsembleSampler(nwalkers,ndim,log_probability,
                    args=(),pool=pool,backend=backend)
    sampler.run_mcmc(pos,nsteps,progress=True)
```